University of South Carolina
Scholar Commons

2014

Timewalk Correction Analysis with FADCs

Saptaparnee Chaudhuri
University of South Carolina

Follow this and additional works at: https://scholarcommons.sc.edu/etd

Part of the Physics Commons

Timewalk Correction Analysis with FADCs

By

Saptaparnee Chaudhuri

Master of Science
University of Bangalore, 2009

Bachelor of Science
University of Delhi, 2007

Submitted in Partial Fulfilment of the Requirements

For the Degree of Master of Science in

Physics

College of Arts and Sciences

University of South Carolina

2014

Accepted by:

Ralf Gothe, Director of Thesis

Steffen Strauch, Reader

Lacy Ford, Vice Provost and Dean of Graduate Studies

Acknowledgements

I thank Professor Ralf Gothe for his guidance throughout the time we worked together. I honestly would not have made it this far if he hadn't helped me in understanding every step of the project.

To my parents, for their everlasting love and emotional support and also for keeping me motivated to fight through difficult times. I owe my accomplishments to them.

To my friend Vineet Garg, for being by my side motivating me and supporting me.

To my colleagues Cameron Nickle and Aneta Netz, thank you for your help with the coding. I could complete my project on time only because of your help with the coding. Thank you too both of you for listening patiently to all the troubles I had with coding. I wish I could get great colleagues like you guys always.

To Gleb Fedokov, thank you for your timely suggestions especially on the time resolution part.

Abstract

The upgraded CLAS12[1] (12 GeV) detector is built around a six-coil toroidal magnet that divides the active detection area into six azimuthal sectors. The Forward Time-of-Flight system (FTOF) is a major component of the CLAS12 detector. It is used to measure the time-of-flight of the charged particles emerging from the interaction of the probing particle with the target. In each of the six sectors of the CLAS12, the FTOF system is comprised of three arrays of counters referred to as panel-1a, panel-1b, panel-2b. Panel-1b arrays consists of 62 counters each and was built at USC. This research focuses on the "timewalk correction" analysis of the timing signals from panel-1b counters with the help of FADC250 (flash adc) information, where the integrated charged is measured in 4 ns intervals with clock frequency of 250 MHz. "Timewalk correction" attempts to correct for the systematic timing shift introduced by the leading edge discriminators. Signals from FADC250 generally follow a Landau distribution. The signals from the PMTs have the same time of arrival, reach their maximum amplitude remain the same time, but the time at which they cross the threshold of the discriminator varies (see Figure 4.12). With the known threshold voltage of the Leading Edge Discriminator (20 mV) the difference in time between the maximum amplitude of the signal and the threshold can

---

[1] CEBAF Large Acceptance Spectrometer

be determined. Three-bar cosmic ray method has been followed to determine the time resolution of the scintillator counter using the corresponding TDC values. The results have been compared with the standard timewalk correction method applied and developed by our group. The timewalk-uncorrected time resolution was measured to be 87 ps as compared to 86.6 ps by standard method. However the timewalk-corrected time resolution was 85.4 ps as compared to 42.6 ps by standard method. FADC250 did not provide significant effect on the time resolution after timewalk correction the reason of which has been explained in Chapter 6.

Table of Contents

List of Figures

Chapter 1: Introduction

The CLAS (CEBAF[2] Large Acceptance Spectrometer) detector in Hall B at Thomas

Jefferson Lab (JLab), Virginia is unique in a way that it has very large acceptance. The

momentum and the angles of almost all the particles produced in an electron proton

collision process can be measured. The detector is roughly spherical in shape and it

measures 30 feet across. It completely surrounds the target, which is typically a small

vial of liquid hydrogen or deuterium. With the 12 GeV electron energy upgrade at Jlab,

the CLAS detector needs to be upgraded too.

 D.S Carman, 2013[1] states that the CLAS12 detector is built around a six-coil toroidal

magnet that divides the the detection area into six azimuthal regions known as sectors.

The toroidal coils are approximately planar in shape and each sector subtends an

azimuthal angle of 60 degrees from the mid-plane of one coil to the mid-plane of the

adjacent coil. The mid-plane of the sector is an imaginary plane that bisects the azimuth

of each sector. The detector has successive layers of sub-detectors. As the particles

produced after the collision fly out of the target, their paths are bent by the detector's

---

[2] Jefferson Lab's main research facility is the CEBAF accelerator. This accelerator consists of a polarized electron source and injector and a pair of superconducting RF linear accelerators. Its energy has now been upgraded to 12 GeV. CEBAF accelerator has been designed such that it allows the electron beam to be continuous rather than producing a pulsed beam. The continuous electron beam produced by the accelerator is one of the distinguishing features of CEBAF. When a nucleus in the target is hit by an electron beam, an "event" occurs which results in scattering of particles into the detector. Each Hall consists of an array of particle detectors that can track the physical properties of the particles produced by the event. The signals from the detectors are then sent to ADCs and the TDCs.

magnet. The particles first enter the wire chambers which measures the curved paths of these particles and hence the momentum of the particles is determined.

The next detector layer is the Forward Time-of-Flight system (FTOF) and it measures the time-of-flight of the charged particles produced in the electron-target collision. The average path length from the target to the FTOF counters is roughly 7 m.

The system specifications for the FTOF require an average time resolution of 80 ps at the more forward angles of CLAS12 and 150 ps at angles larger than 35°. In each of the six sectors of CLAS12, the FTOF system is comprised of three arrays of counters, referred to as panels: panel-1a, panel-1b and panel-2.

Each panel consists of rectangular scintillators with a photomultiplier tube (PMT) glued to each end. Panel-1s refer to the counters located at forward angles 5° to 35°. Both the panels 1a and 1b are required to meet the average time resolution of 80 ps. Panel-2 refers to the counters at larger angles 35° to 45°. Each of the six panel-1a arrays consists of 23 counters. The panel-1b arrays consist of 62 counters each and each of panel-2 array consist of 5 counters each. Once the momentum and the velocity of the particle are known, its identity can be found. The CLAS12 detector also contain Cherenkov Counters (CC) and Electromagnetic Calorimeter (EC) which distinguish electrons from the other types of particles.

(a) Particle separation.

(b) Resolution curves.
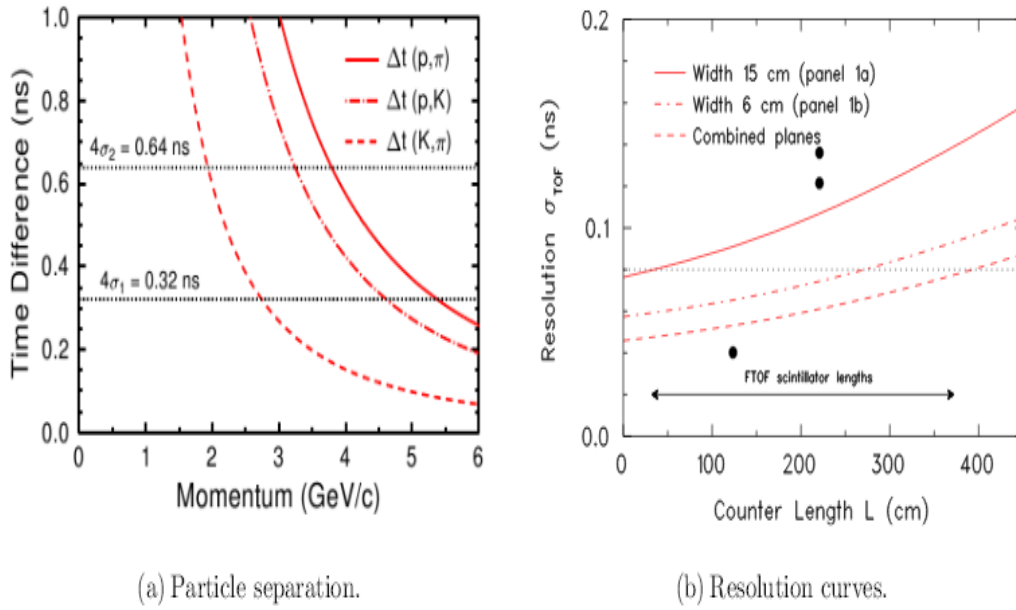
Figure 1.1: Particle separation and resolution curves.

(a) The three curves indicate the time of flight differences, between the p/π and π/K over 650-cm path length from target to panel-1b. σ_2 corresponds to panel-1a counters; σ_1 corresponds to panel-1b counter. (b) The data point at (120 cm,40 ps) indicate a typical cosmic ray resolution measurement of panel-1s at University of south Carolina, whereas (213 cm,138 ps) refers to the resolution of panel-1a counter from JLab as measured at University of South Carolina in 2009.

According to **Ralf Gothe, 2009[2]** , "the time-of-flight subsystem of the CLAS detector in Hall B was designed to allow separation of pions and kaons in the kinematic range accessible with a 6-GeV electron beam by providing time resolutions from 90 ps to 160-ps at the forward angles, where the most energetic particles are detected. To reliably

separate p, π and K in the kinematic range accessible with the proposed 11-GeV beam of the CEBAF upgrade, the FTOF detector must achieve a resolution of 80 ps as illustrated in Figure 1.1. This assumes a 4σ time difference between two particles, thus allowing for identification of a signal in the presence of other particles with a ten-fold higher rate. As in the old 6-GeV FTOF detector (Panel 1a), each counter of the new additional 12-GeV FTOF (Panel 1b) is composed of a long rectangular plastic scintillator with two cylindrical PMTs, one on each end, directly attached without light guides. The scintillator lengths are tightly constrained by the established six-panel FTOF geometry and the requirement that the new panels do not restrict the CLAS12 acceptance as defined by the other detector components, but the thicknesss and the width, 6 cm x 6 cm, are selected to optimize photon statistics, geometric matching with the photocathodes, and the closest possible stacking. Compared to the Panel-1a 5 cm x 15 cm FTOF scintillators, the 6 cm x 6 cm scintillators increase the number of photons produced by a factor of 6/5; the increased ratio of photocathode area to the scintillator exit window area increases the number of photons that reach the photocathode by at least a factor of 25/12. This increases the number of photons reaching the photocathode by a factor of about 5/2 and, therefore, improves the resolution by a factor of $\sqrt{2/5}$, neglecting the resolution of any contributions that are independent of light level.

 With a time resolution of better than 150 ps for the longest counters of Panel 1a, the Panel-1b counters must achieve resolutions of better than 95 ps for the combined resolution goal of 80 ps to be reached (Figure 1.1). The final panel-1s results exceed this requirement.

4

Figure 1.2: CLAS12 detector system[3].
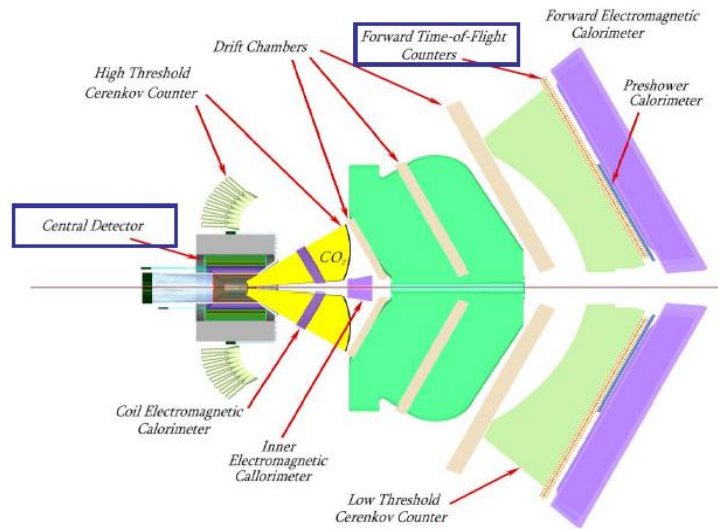
The main components of the CLAS12 detector system are the toroidal magnet, Drift

Chambers (DC), Cherenkov Counters (CC), Time-of-Flight Detectors (TOF),

Electromagnetic Calorimeters (EC). The Forwad Time-of-Flight panel-1 counters are new

features added to the already existing TOF subsystem.

---

[3] The figure shows a mid plane cut through of the upgraded CLAS12 detector system.
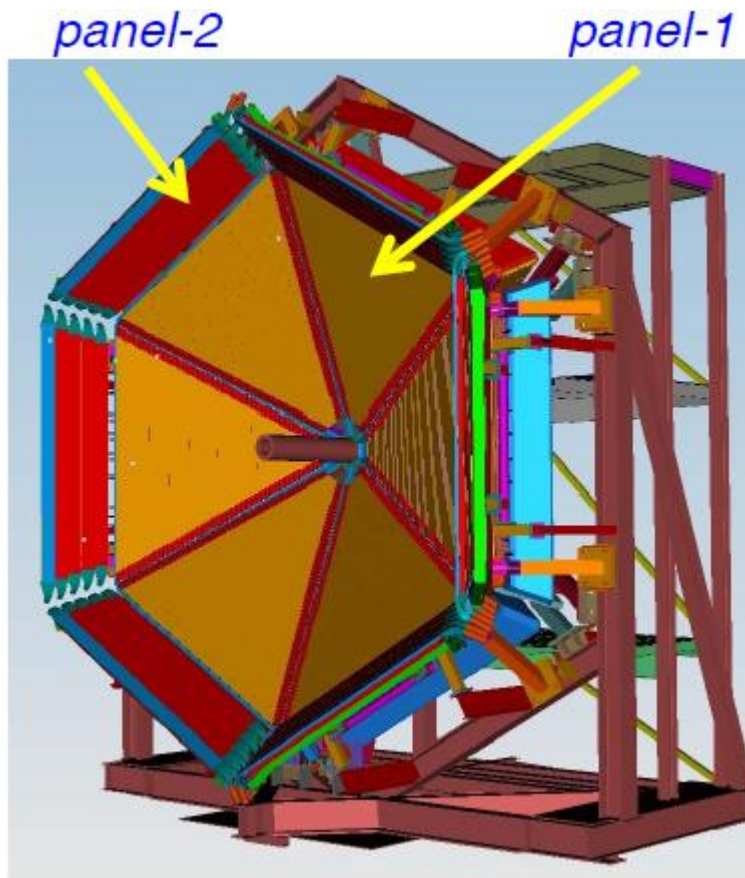
Figure 1.3: The panel-1 and panel-2 of the FTOF system.

 FTOF consists of 3 scintillator panels in each CLAS12 sector. Panel-1a is the original CLAS

panel-1. Panel-1b consists of new counters with better time resolution (combined 80 ps)

and panel-2, which is the original panel-2. The good time resolution of the panel-1s cold

be achieved after optimized "timewalk" corrections developed and applied by our

group.

 The anode signals from photomultiplier tubes (PMT) are used for timing and the

dynode signals are used for ADC measurements. The anode signals are transformed into

logic signals by Leading Edge Discriminators. The logic signals are then sent to the

coincidence module. A coincidence output signal is produced if any part of the incoming

6

signals overlaps. All pulses arriving within a time equal to sum of their widths are registered as coincident. Flash ADC model FADC250 information has been used for time-walk correction (Figure 4.12, Chapter 4) of the TDC signals from the panel-1b counters. As referred to **FADC250 [3]**, FADC250 provides 12-bit data words streaming at 250 MHZ and integrating the charge from 16 ADCs. Samples from the ADC are immediately subtracted from a programmable pedestal before any further processing. The result is however not allowed to go below zero. The pedestal value is different for different ADCs.
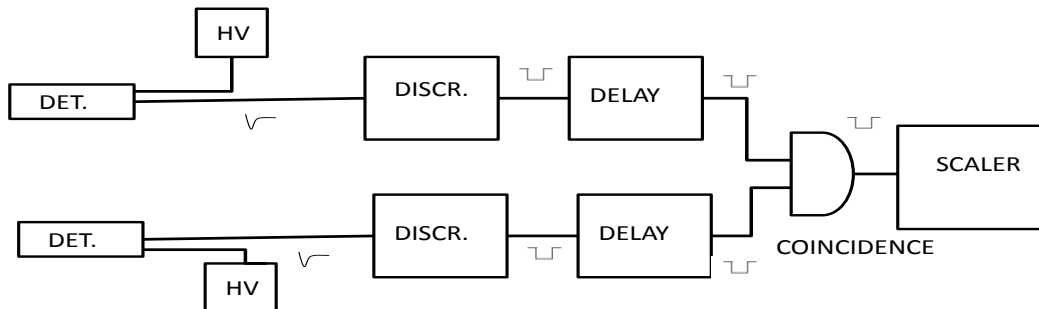

 Figure 1.4: A typical coincidence circuit.
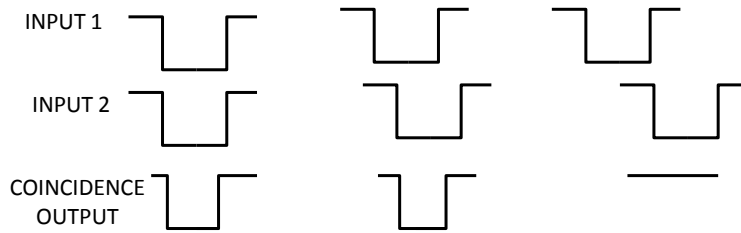
Figure 1.5: Coincidence between two pulses.

The circuit diagram in Figure 1.4 shows a simple coincidence circuit with two signals. This is just a general description of the working of a coincidence module. In order for this circuit to work it is necessary that the electrical path of each branch leading to the coincidence module be of equal length. This can be achieved by adding adjustable delays to each line as shown in the Figure 1.5. An "event" requires a 12- fold coincidence of all the twelve PMT signals. The threshold of the discriminator is kept at a low value so that the discriminator can register the low energy deposits. The threshold for the Leading Edge Discriminator in this case is kept as low as 20 mV.

8

Figure 1.6: Electronic configuration at USC[4].

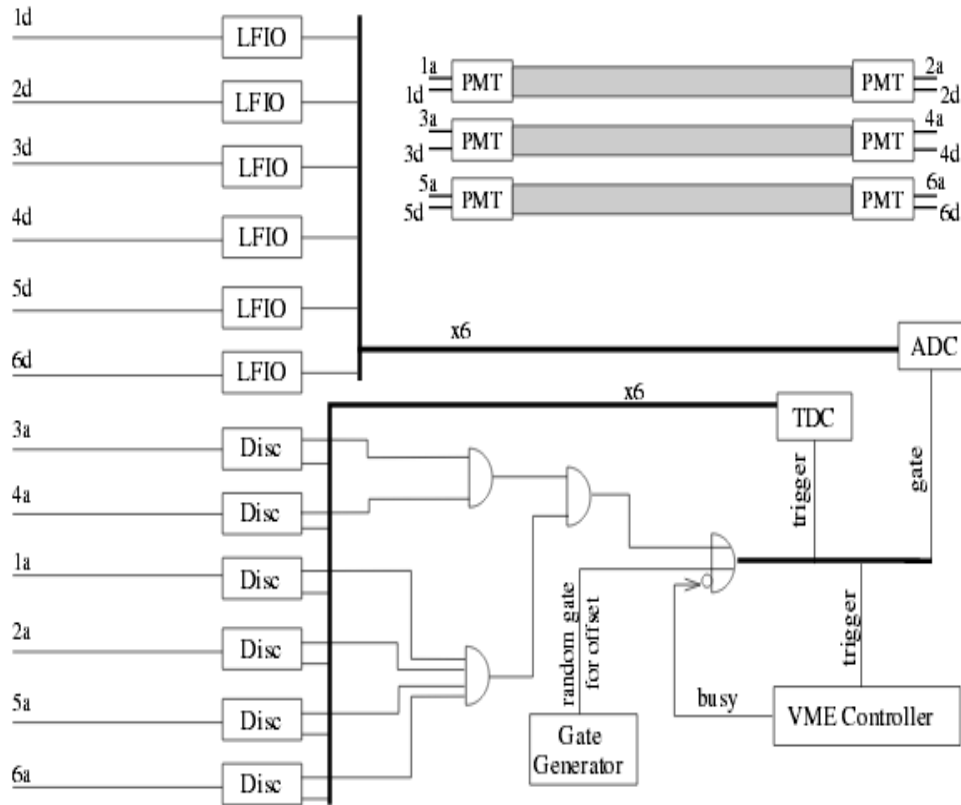Figure 1.6 shows the circuit used at USC and a 3-bar cosmic ray method was followed to determine the time resolution. As referred to *Ralf Gothe[2]* Figure 1.6 shows that each dynode signal passes through a Linear Fan-In/Fan-Out (LFIO). The anode signals from the PMTs are transformed into NIM logic signals by LeCroy 623B Leading Edge Discriminators, and the coincidence circuit is provided by Phillips Scientific (PS) 755 Quad Logic and LeCroy 622 Coincidence units. The six-fold final coincidence triggers theVME modules. The V1290N pipeline TDC used in the circuit is then triggered to record signals arriving from the discriminators. At USC we have used instead of the FADC250, V792N QDC that receives 100 ns integration gate in which all the signals of the event arrive.

---

[4] As referred to Ralf Gothe[2], "The six PMTs of the three counters are labeled 1-6 from the top left to the bottom right. Each provides an anode and dynode signal, labeled as a and d, respectively. The six-fold coincidence is setup so that PMT 3a, the middle-left PMT, provides the reference time."

9

Chapter 2: Plotting the ADC Distribution Signals

In this work we analyse the data from FADC250 had a total of 85005 events numbered from 1 to 85005. There were a total of 12 x 100 over 4 ns integrated values of FADC and 12 TDC (timing) signals one from each PMT (as mentioned there are a total of 12 PMTs). Each PMT had one value of fully integrated FADC and TDC signals with 100 different raw amplitudes (ADC_raw) from the FADC250 taken at 4 ns interval. A typical plot of the charge distribution against time is shown in the Fig. 2.1 for event number iev= 30.
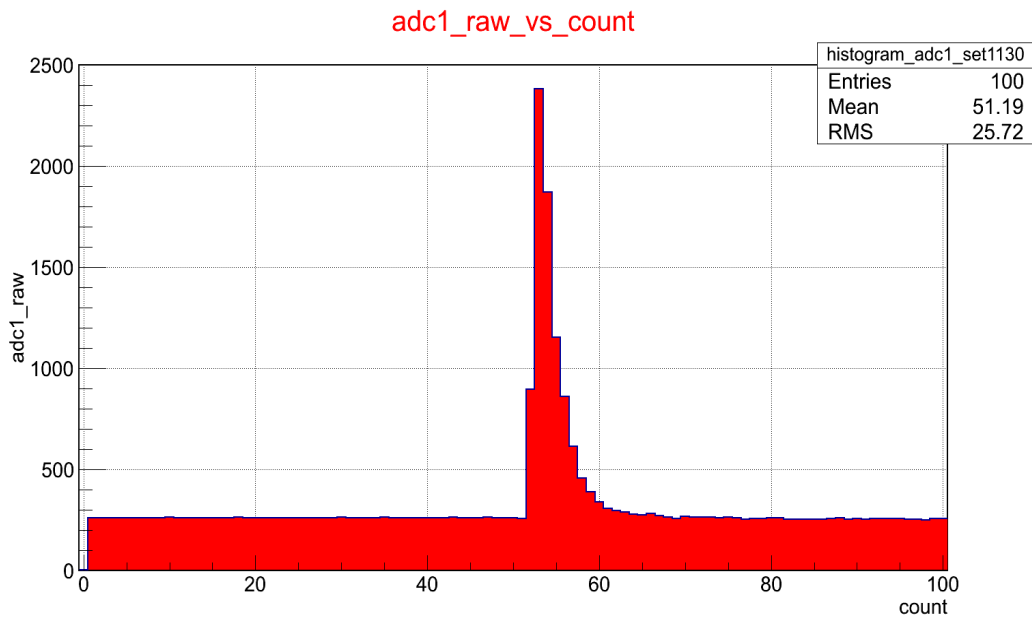

Figure 2.1: FADC250 distribution against time.

In Figure 2.1, the charge distribution shows a Landau distribution. On the y-axis the charge distribution is 100 fC per channel. On the x-axis the time is 4 ns per channel. The histogram is not offset subtracted so that it is about 250 y-axis channels above zero. The maximum amplitude of the signal is around 2500 y-axis channels which is 250 pC of 4 ns integrated charge.
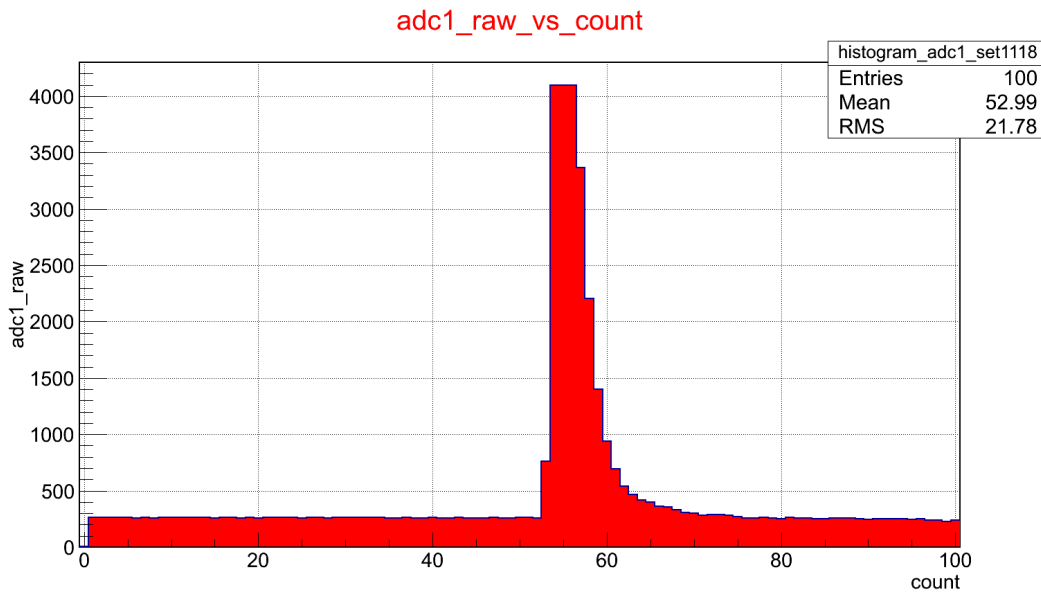
Figure2.2: The FADC250 charge distribution of large signal from PMT 1.

The histogram in Figure 2.2 is again not offset subtracted and the maximum amplitude reaches to around 4000 y-axis channel i.e 400 pC of charge. The flat top of the histogram shows that the charge distribution has reached digitization maximum (400 pC). The maximum charge that could be recorded is 4096 y-axis channels i.e. about 400pC.

Initially the histogram offset of the charge distribution against time was at approximately at 250 channels above the zero on the y-axis. The integral of the x-axis

11

bins starting from 0 to 40 was calculated and then this value was divided by the total

number of bins in this range so as to get the average value per bin. This calculated

average value was then subtracted from each bin of the existing histogram so as to bring

the histogram to zero. The offset subtracted histograms had maximum amplitudes

ranging from 1500 y-axis channels (150 pC) to 4000 y-axis channels (400 pC).
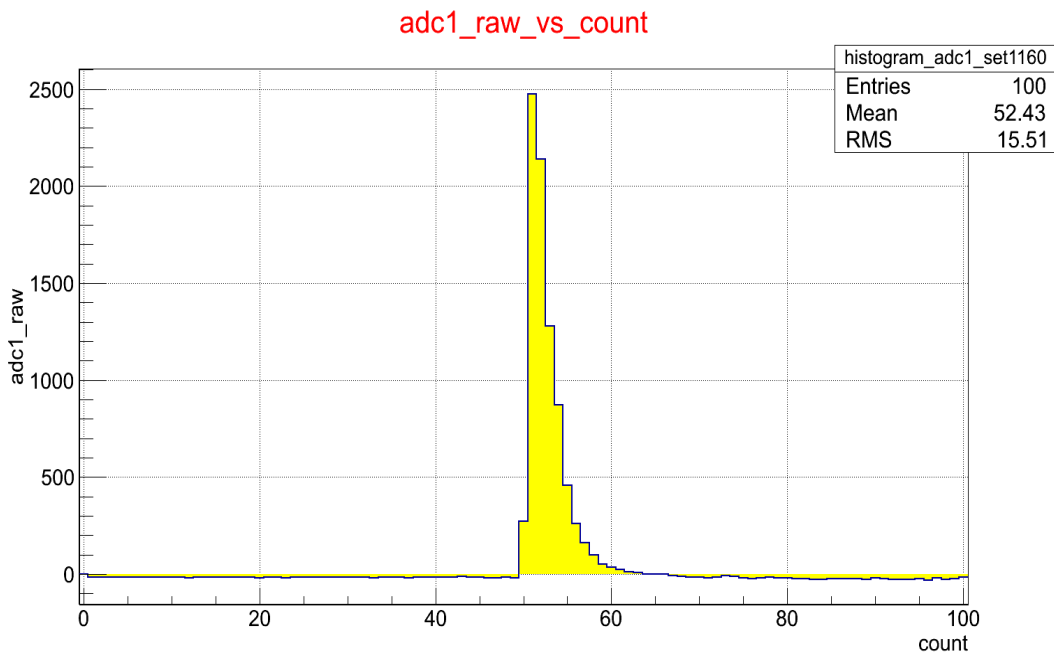
Figure 2.3: FADC250 charge distribution from PMT 1 after offset subtraction.

  The histogram in Figure 2.3 has been offset subtracted. This is an example of the

charge distribution where the amplitude reaches around 2500 y-axis channels i.e. only

25 pC. The events with such low amplitude signals were not selected when the total ADC

integral (over all 85005 events) range was set between 1000 to 17000 x-axis channels

(10 pC to 170 pC) to avoid signals of particles not passing through at least 6 cm of

scintillation material (Figure 2.3) and too large signals of particles passing through at a

too flat angle (Figure 2.4) .

12

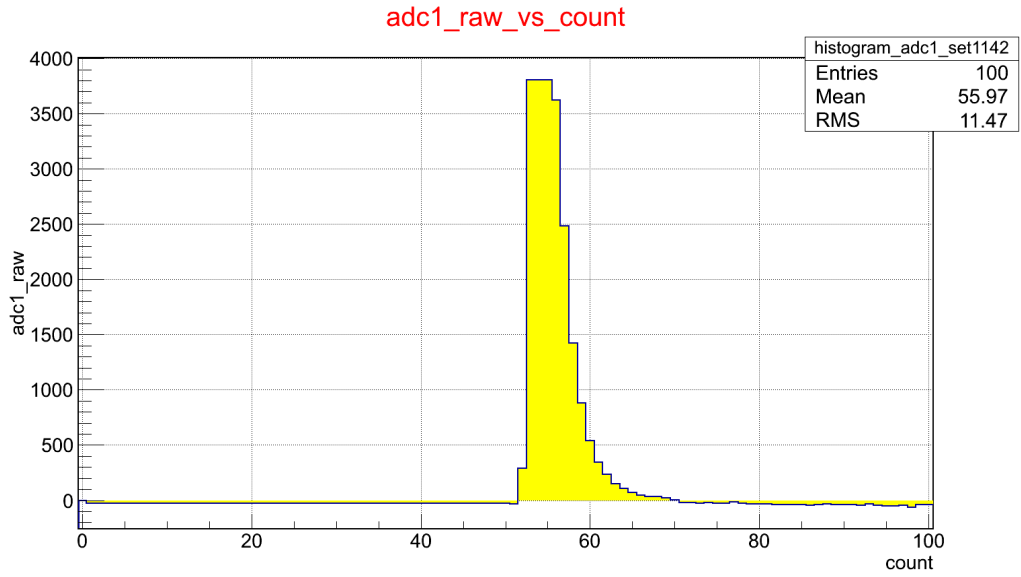**Figure 2.4:** **Histogram with maximum charge of 400 pC with offset subtraction.**
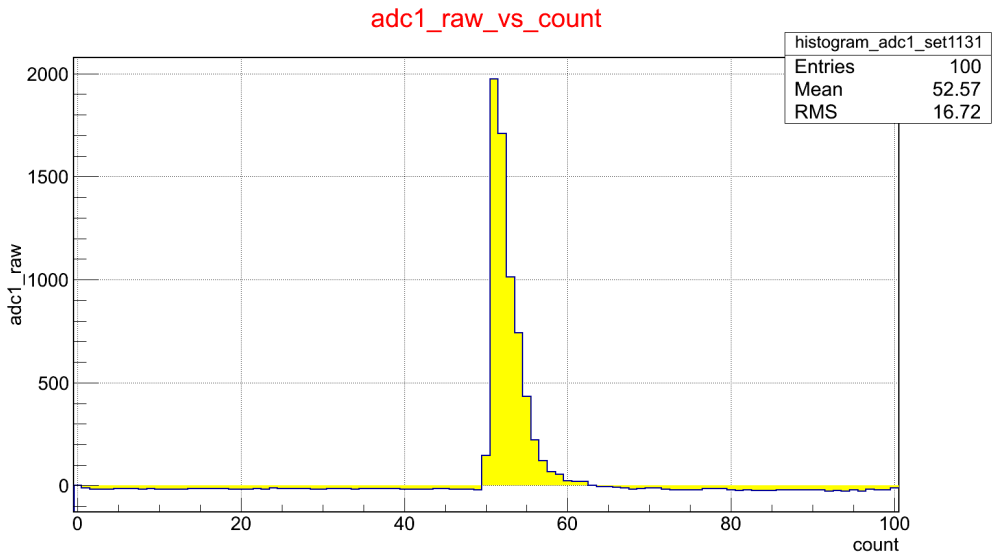
Figure 2.5: Typical example of the FADC250 charge distribution from PMT1.

Figure 2.5 shows the maximum amplitude for a typical histogram in Figure 2.5 is 2000

y-axis channels i.e. 200 pC
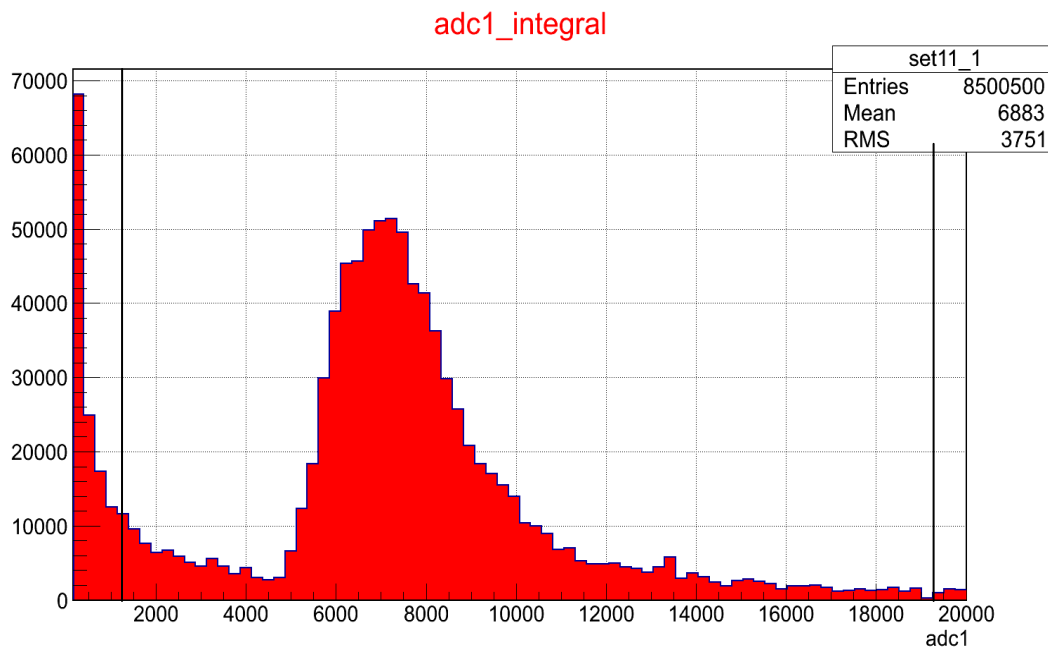
Figure 2.6: Histogram of the full integral values of FADC1.

The selection of the good events was done selecting the range of the integral values

over all 85005 events of the ADC distribution. In this case the lower integral limit is 1000

x-axis channels and the upper integral limit is 17000 x-axis channels as shown by the

black lines. Selection of the lower and the upper values of the ADC integral values

exclude the events with very low signal amplitude and the signals with maximum value

of the charge distribution greater than 400 pC.

There are certain histograms where there is no charge distribution (offset only) as in Figure 2.7.

Figure 2.7: FADC250 distribution against time with flat signal.

The FADC distribution from PMT 1 is shown and count represents the time intervals with 4 ns per channel. This particular event in Figure 2.7 displays no signal (no Landau distribution of charge). However by putting a lower limit in the FADC integral value these events were excluded.
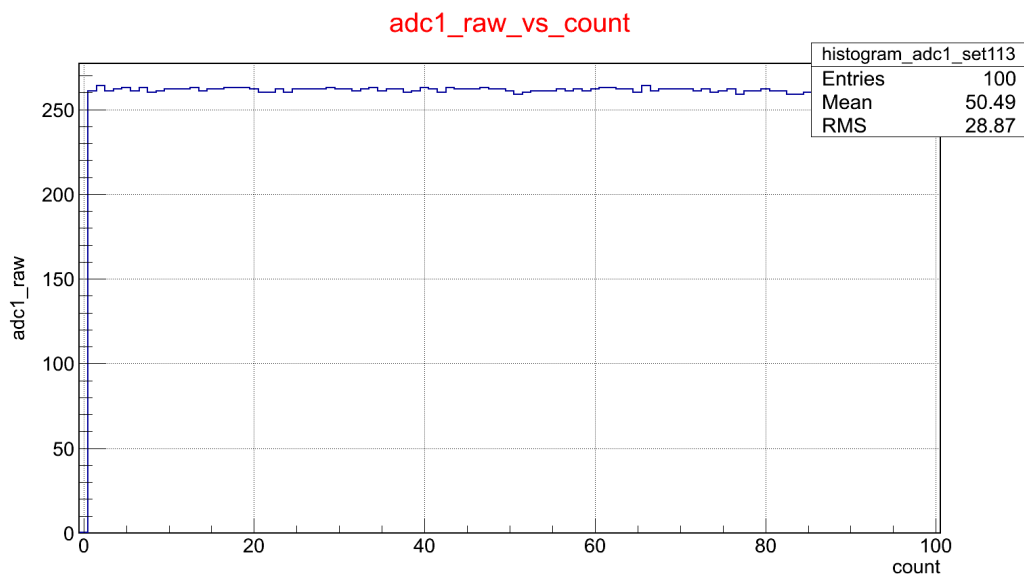
Chapter 3: The Fit Function

 The ADC distribution histogram has the shape of a Landau distribution function. After

the offset subtraction the histograms were fit by a Landau distribution function. The

ultimate goal in fitting the histogram is to extract the parameters from the histogram

that would be used to calculate the risetime of the PMT signals and the delay in the

timing signals in order to correct for the timewalk. It was an important part of this work

to fit the histogram with a proper function that can represent the original signal. In

order to check if the fit works well the value of the reduced chisquare is calculated for

each fit. The reduced chisquare is the ratio of the chisquare value got from the fit and

the number of degrees of freedom. If the value for the reduced chisquare is close to 1

then the fit works best. However in my case not all fits had the reduced chisquare value

close to one but typically between 0.5 to 40.5 .

16
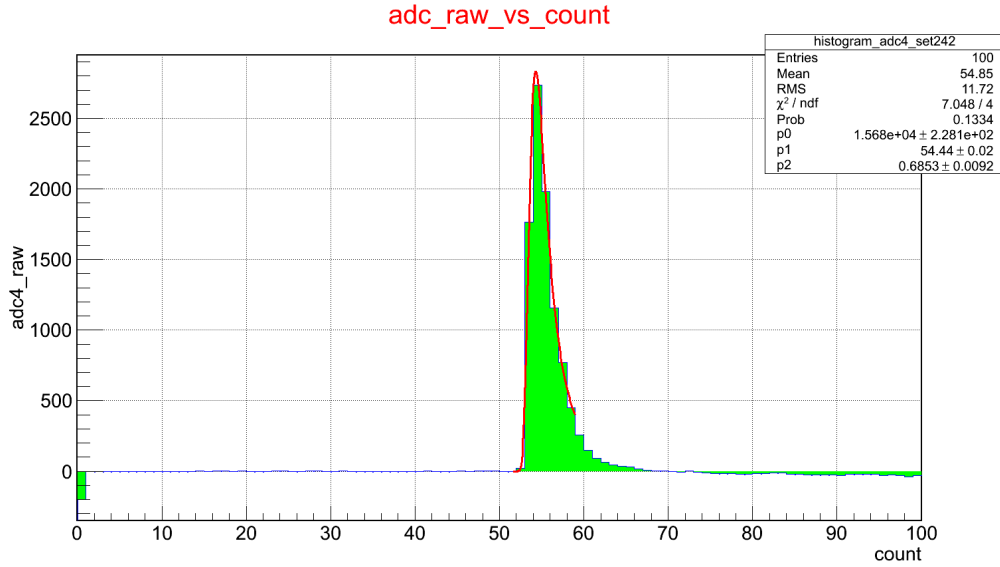
Figure 3.1: FADC distribution histogram fit by a Landau function.[5]

Figure 3.1 shows an example, where the reduced chisquare value for this histogram is

1.762.
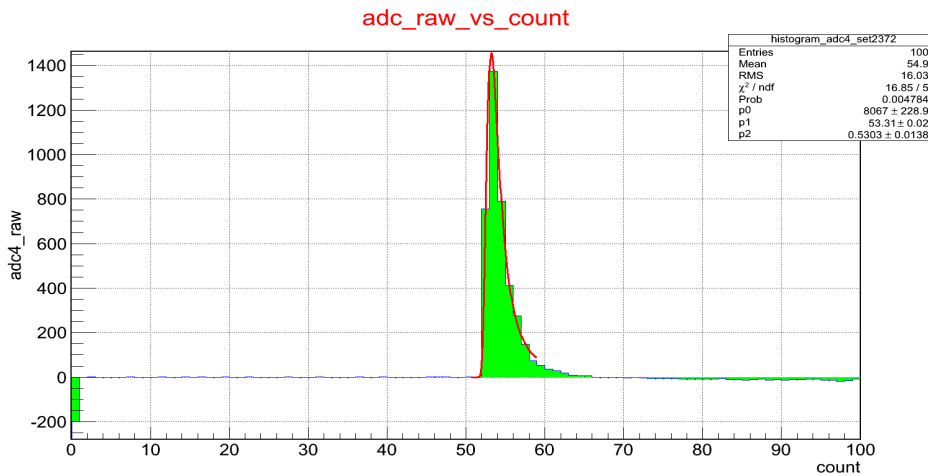
Figure 3.2: Another example of the fitted FADC distribution histogram.

Figure 3.2 shows another example FADC histogram fitted by a Landau function. The

reduced chisquare value for this case is 3.37.

---

[5] Shows variations of the reduced chiquare values with the fit function.

17
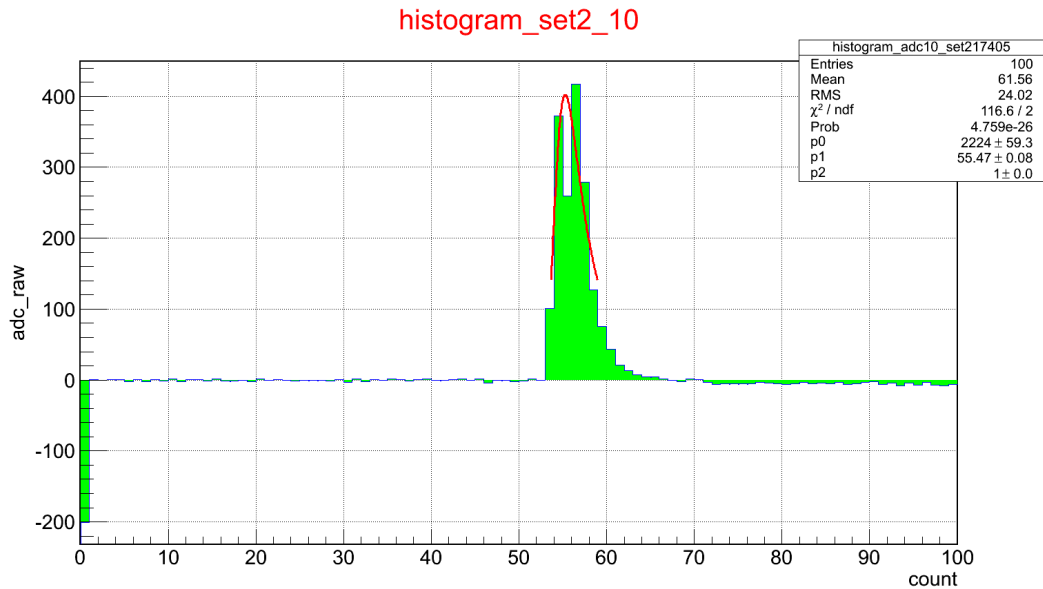
Figure 3.3: A distorted FADC distribution histogram. [6]

Figure 3.3 is an example of a distorted charge distribution of a PMT noise signal that is

not generated by the particles passing through at least 6 cm of scintillation material. The

Landau fit does not work for this case and hence the reduced chisquare value is 58.3.

---

[6]Before proper event selection there are many events for which the signals are distorted. The reduced chisquare value for these fits are very high. But these events are eventually excluded before doing further calculations.
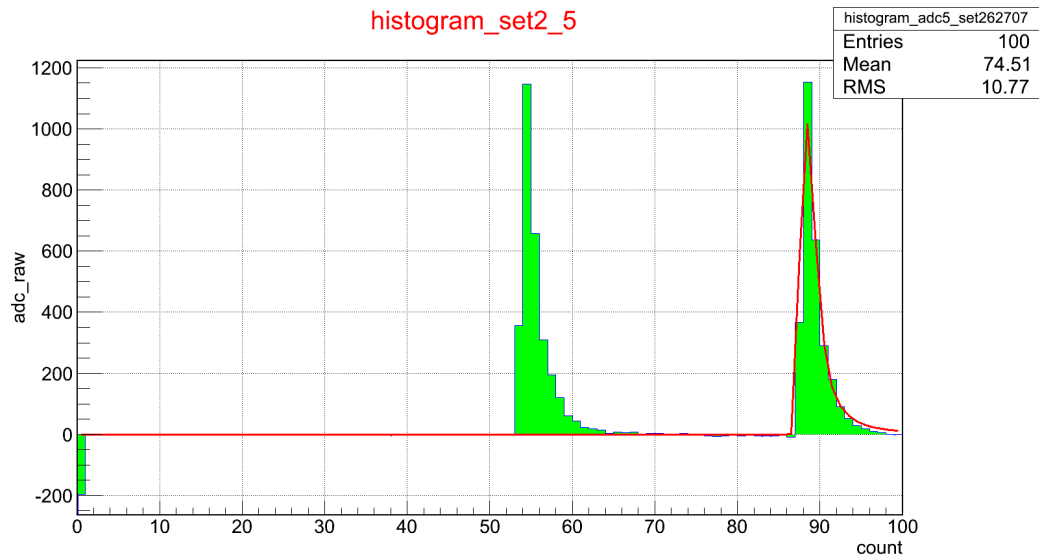
Figure 3.4: Two signals in a single event.

Figure 3.4 shows an example where two signals appear in a single event. The fit function did not work in such cases as well so this particular event was not considered for further calculations. This is in fact a very rare event when two signals are recorded for a single event. The timing of the signals here are 120 ns (4 ns per x-axis channel) apart, so one cannot conclude that they are from the same cosmic ray hitting the counters.

19

Chapter 4: Risetime checks on the histograms

After the fit, risetime checks on the histograms were conducted. Two different risetime checks are commonly defined. The time required for the signal to rise from 10% to 90% of its maximum amplitude was calculated as well as the time required for the signal to rise from 30% to 70% of its maximum amplitude. From the fit function the maximum value of the charge distribution (the signal amplitude) along the y-axis and the corresponding x- axis values (time) x-max could be calculated. Once the corresponding fractions of the maximum amplitude and the corresponding x-values (time) was obtained. The risetime was the difference in time of these x-axis values. The smaller the risetime, the better would be the time resolution. The histograms explain in this section how the rise times were calculated.

adc_raw_vs_count

histogram_adc4_set242	
Entries	100
Mean	54.85
RMS	11.72
χ^2 / ndf	7.048 / 4
Prob	0.1334
p0	1.568e+04 ± 2.281e+02
p1	54.44 ± 0.02
p2	0.6853 ± 0.0092

MAXIMUM AMPLITUDE y_{max}

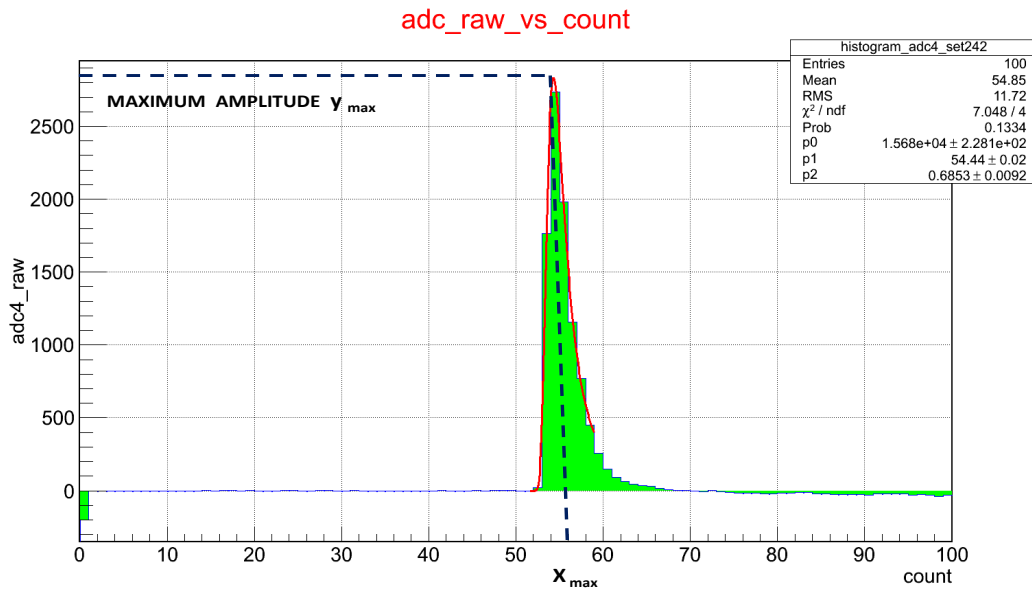x_{max}

count

Figure 4.1: Finding the maximum amplitude.

Figure 4.1 shows how to get the value for the maximum amplitude of the Landau fit function y_{max} and the corresponding x_{max} from a FADC histogram. This code written to fit the signal helps in calculating the value for the maximum amplitude for the signal which is basically the maxim amplitude for the fit function itself.
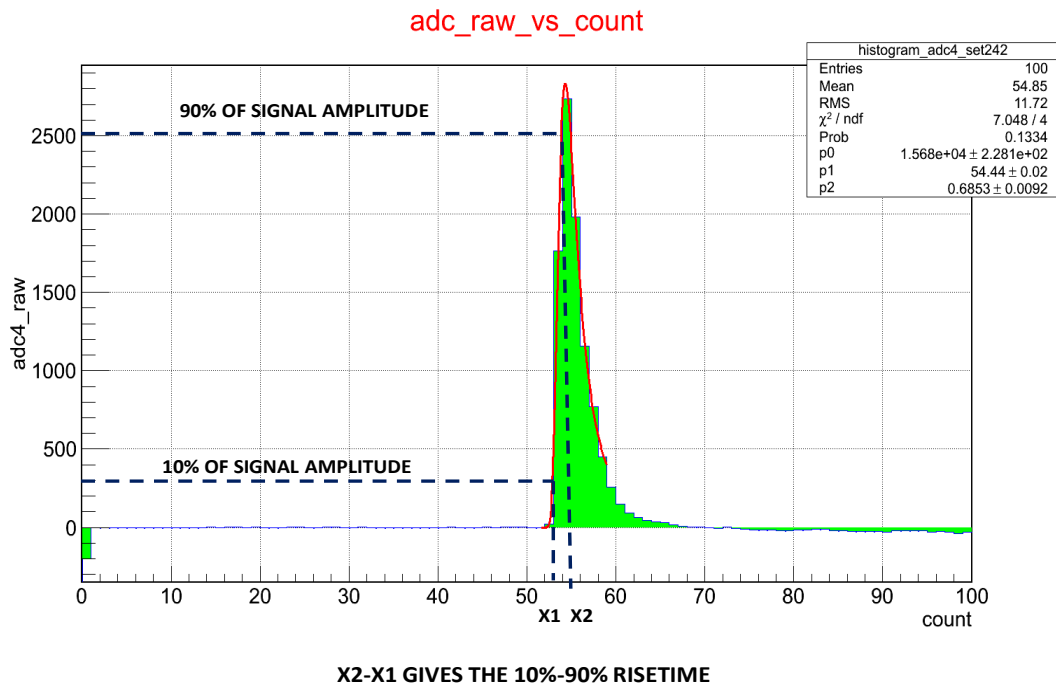
21

Figure 4.2: 10%-90% risetime check for the signal.

Figure 4.2 shows an example of how to calculate the 10% and the 90% of the maximum amplitude for the signal. X1 and X2 are the corresponding values of the 10% and 90% of the maximum amplitude of the signa, respectively. The difference X2-X1 gives the time required for the signal to rise from 10% to 90% of its maximum amplitude.

adc_raw_vs_count

histogram_adc4_set242	
Entries	100
Mean	54.85
RMS	11.72
χ^2 / ndf	7.048 / 4
Prob	0.1334
p0	$1.568e+04 \pm 2.281e+02$
p1	54.44 ± 0.02
p2	0.6853 ± 0.0092

70% 0F SIGNAL AMPLITUDE

30% 0F SIGNAL AMPLITUDE

X3 X4

X4-X3 GIVES THE 30%-70% RISETIME
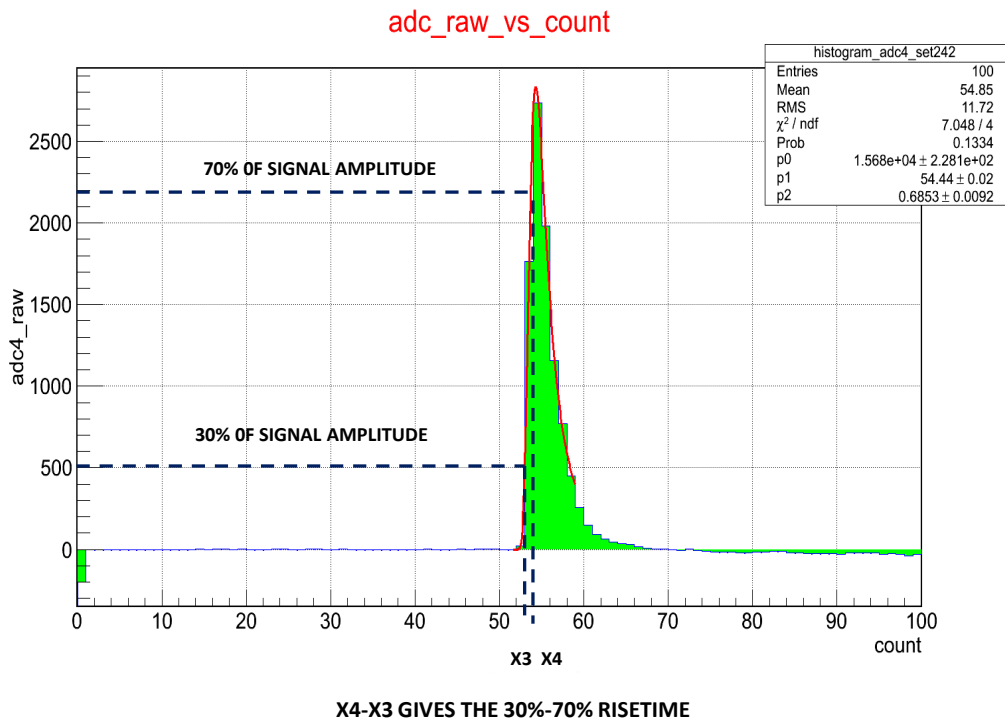
Figure 4.3: 30%-70% risetime check for the signal.

Figure 4.3 shows an example of calculating the 30% and the 70% of the maximum amplitude for the signal. X3 and X4 are the corresponding values of the 30% and 70% of the maximum amplitude of the signal respectively. The difference X4-X3 gives the time required for the signal to rise from 30% to 70% of its maximum amplitude.

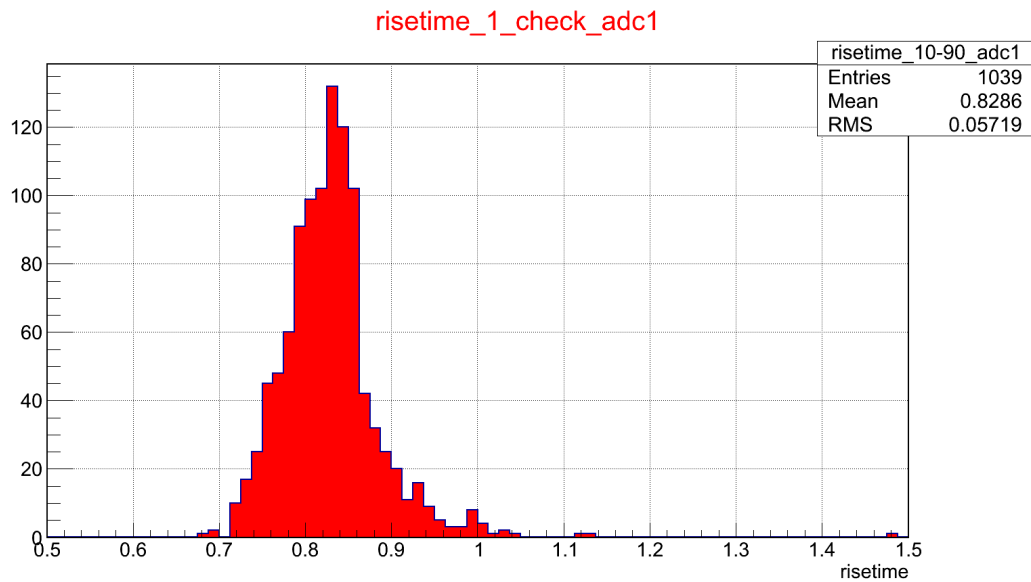**Figure 4.4: 10%-90% risetime check.**

Figure 4.4 shows a one-dimensional histogram for the 10% to 90% risetime check on

the signals from FADC for all events. The risetimes show a Gaussian distribution.

The mean value for the risetime is 3.31 ns.

24

risetime_2_check_adc1

risetime_30-70_adc1	
Entries	1039
Mean	0.3524
RMS	0.02276

Figure 4.5: 30%-70% risetime check.
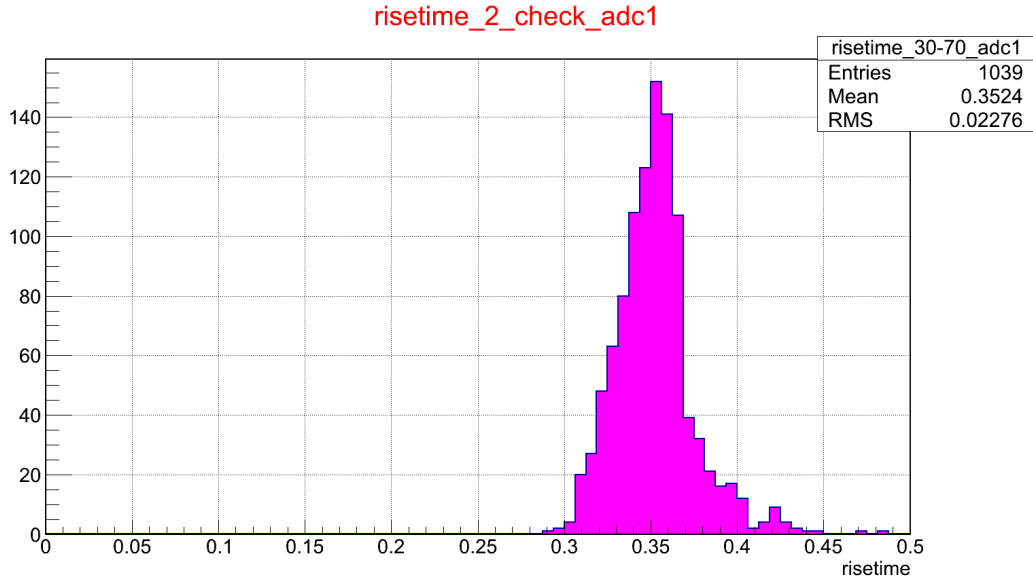
Figure 4.5 shows a one-dimensional histogram for the 30% to 70% risetime check on the

signals from FADC for all events. The risetimes here show Gaussian distribution as well.
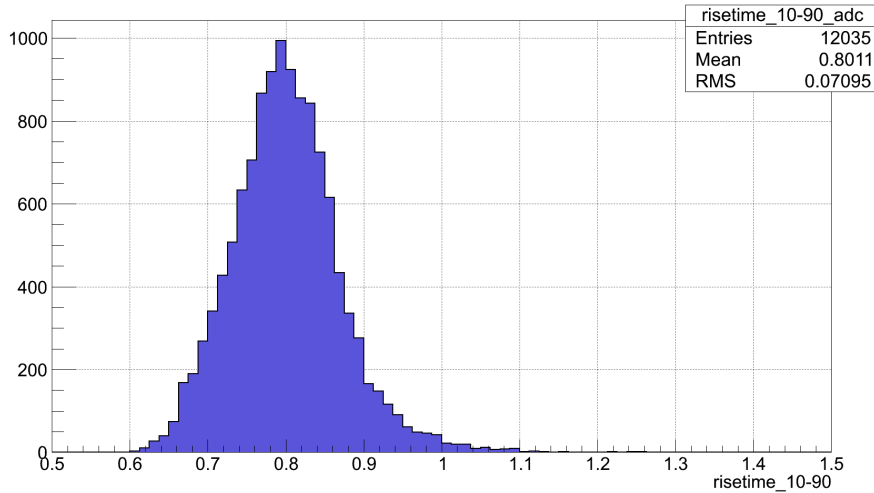
The mean value for this risetime is 1.40 ns.

risetime_10-90_adc	
Entries	12035
Mean	0.8011
RMS	0.07095

Figure 4.6: 10%-90% from FADC1 to FADC12.
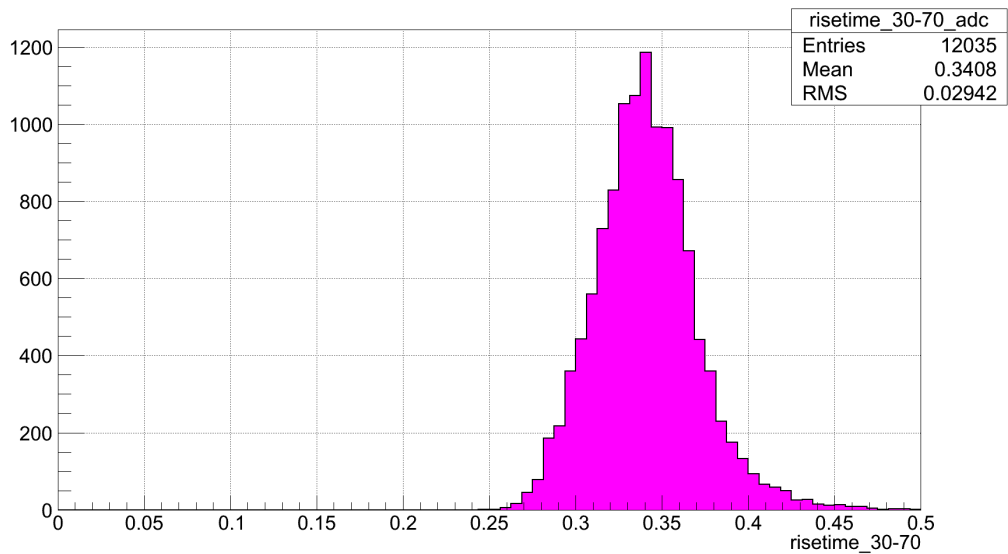
www.manaraa.com

Figure 4.7: 30%-70% from FADC1 to FADC12.

Figures 4.6 and 4.7 show the risetime distribution for all twelve FADCs over all events.

The two one-dimensional histograms clearly show a Gaussian distribution as well with

respective mean values as 3.20 ns and 1.36 ns.

From the Landau fit function that has been used to fit the FADC distribution, the mean

value and the amplitude of the fit function can be determined. The threshold for the

Leading Edge Discriminator in this case is set to be at 20 mV. The x-axis and the y-axis

channels that correspond to the threshold of the discriminator (20 mV) could be

determined from the fit function as well. The difference in values between the x-

channels corresponding to the threshold and the mean value of the fit function as well

as between the threshold and the amplitude of the fit function are illustrated in the

next histograms (Figures 4.8 and 4.9).

X_thr: the x channel corresponding to threshold value
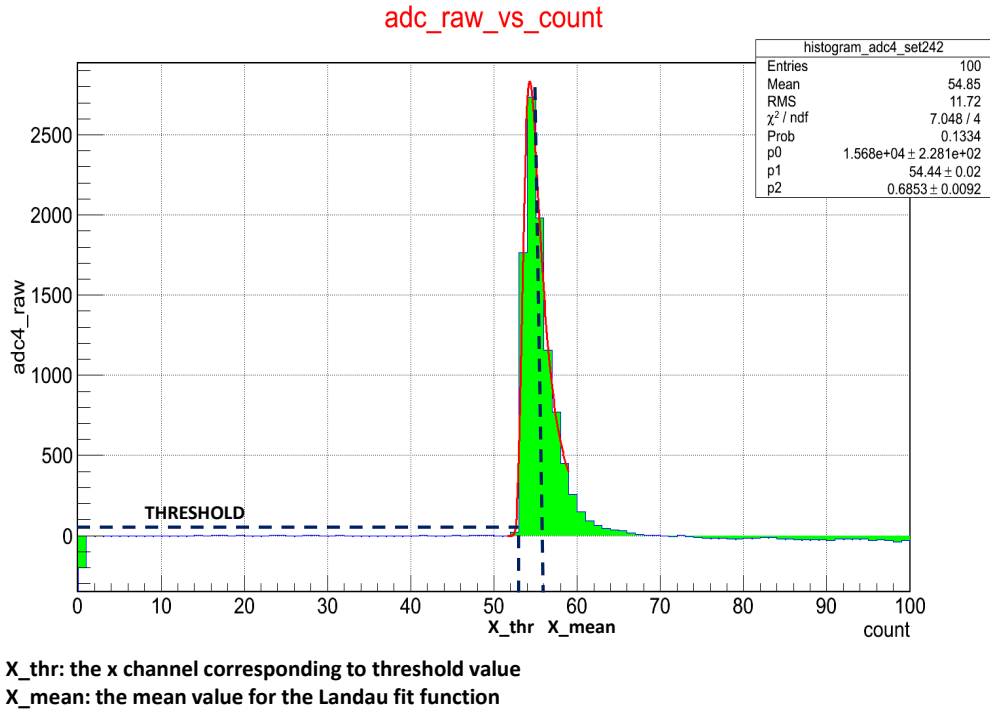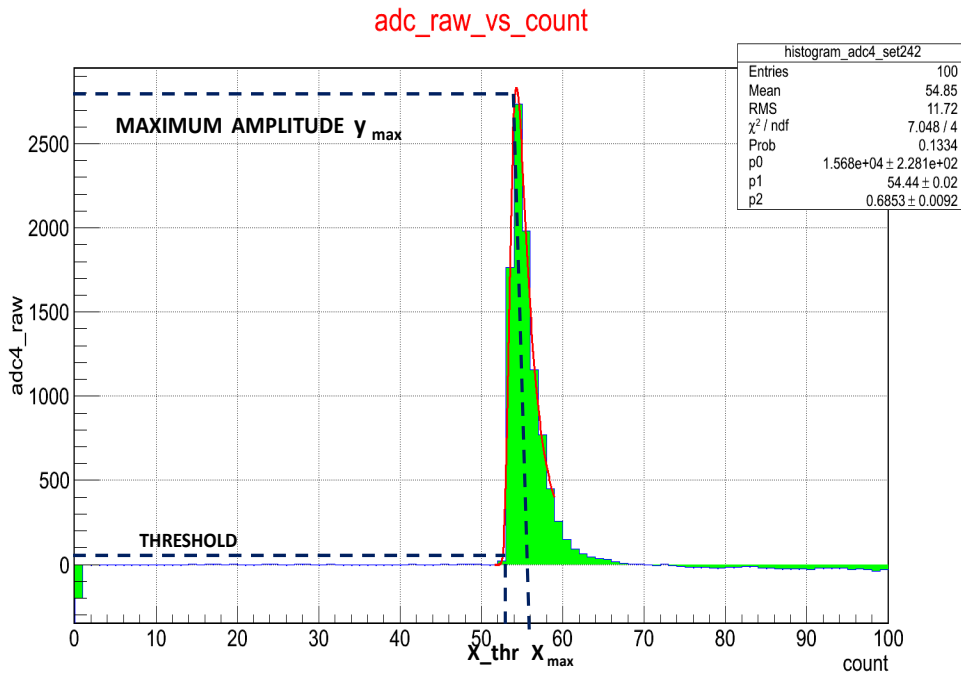**X_mean: the mean value for the Landau fit function**

Figure 4.8: Difference between threshold and mean.

Figure 4.8 shows an example to calculate the difference between the mean value for

the fit function and the threshold value. X_mean-X_thr gives the difference which is

plotted later in a one-dimensional histogram.

27

adc_raw_vs_count

histogram_adc4_set242	
Entries	100
Mean	54.85
RMS	11.72
χ^2 / ndf	7.048 / 4
Prob	0.1334
p0	1.568e+04 ± 2.281e+02
p1	54.44 ± 0.02
p2	0.6853 ± 0.0092

X_thr: the x channel corresponding to threshold value
X_max: the maximum value for the Landau fit function

Figure 4.9: Difference between threshold and maximum value.

Figure 4.9 shows an example to calculate the difference between the maximum value

for the fit function and the threshold value. X_{max}-X_thr gives difference which is plotted

later in an one-dimensional histogram.

These differences between the mean and the threshold and the amplitude and the

threshold have been calculated for all the twelve ADC values. The values of these

differences, found for all twelve ADCs, would be used for timewalk corrections for the
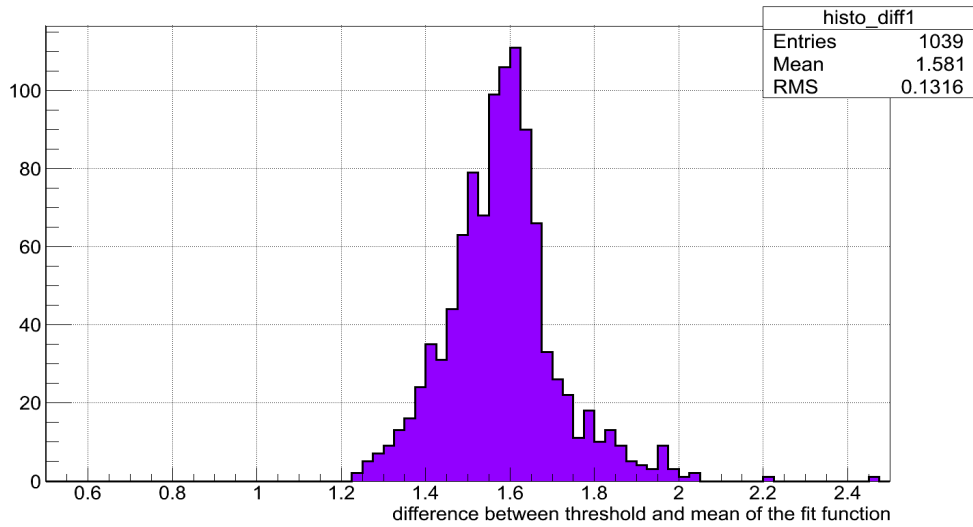
corresponding TDC (timing) signals.

28

Figure 4.10: Histogram of mean minus threshold timing.

Figure 4.10 shows the histogram corresponding to the difference in x-channels (4 ns) between the threshold and the mean value of the fit function for FADC1.
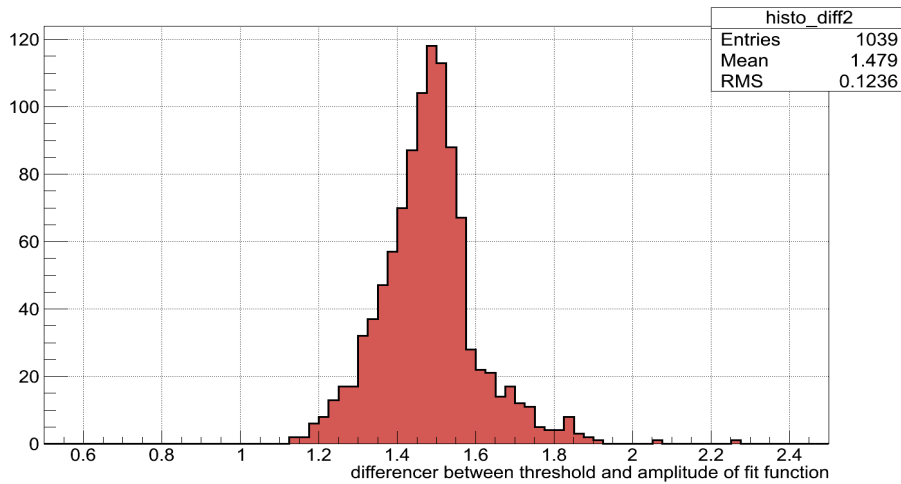

Figure 4.11: Histogram of threshold minus amplitude timing.

Figure 4.11 shows the histogram corresponding to the difference in x-channels between the threshold and the amplitude of the fit function for FADC1.

The mean and the maximum amplitude of the signal do not change in position, but the position of the threshold point changes with respect to the timewalk.
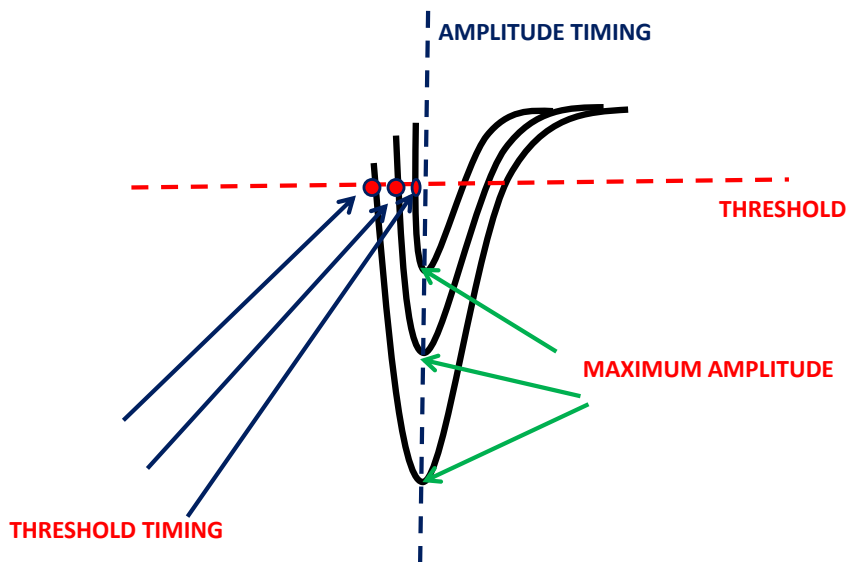

Figure 4.12: FADC signals with varying threshold timing.

Figure 4.12 represents three ADC signals arriving at the same time. The red line represents the threshold of the Leading Edge Discriminator. As shown in the figure the position of threshold point varies according to the timewalk, but the maximum amplitude remains at a fixed position for all signals and so does the position of the mean (not shown in the figure). Hence the difference between the threshold and the

30

maximum amplitude or between the mean and the threshold timings can be used to correct the timewalk.

Chapter 5: TDC Correlations

A TDC or time-to-digital converter digitizes the time of pulses from the photomultiplier tubes. A photomultiplier pulse is transformed in to a logic signal by a Leading Edge Discriminator and its time of arrival is measured by a TDC.

The data files from the 6-bar arrangement at JLab have FADC250 has twelve values of the TDC marked from tdc1 to tdc12 corresponding to the ADC values.

In order to understand the correlation between the TDC values, one needs to understand the arrangement of the six scintillators in the FTOF test system (see Figure 5.1). The clock interval of the pipeline TDC in this case is 25 ps. The diagram in Figure 5.1 sketches the arrangement of the bars and the corresponding PMTs attached at the end of the bars. As explained earlier, each PMT has a corresponding ADC integral value for all events. At first one-dimensional histograms are plotted between the differences of the TDC values for the corresponding PMTs.
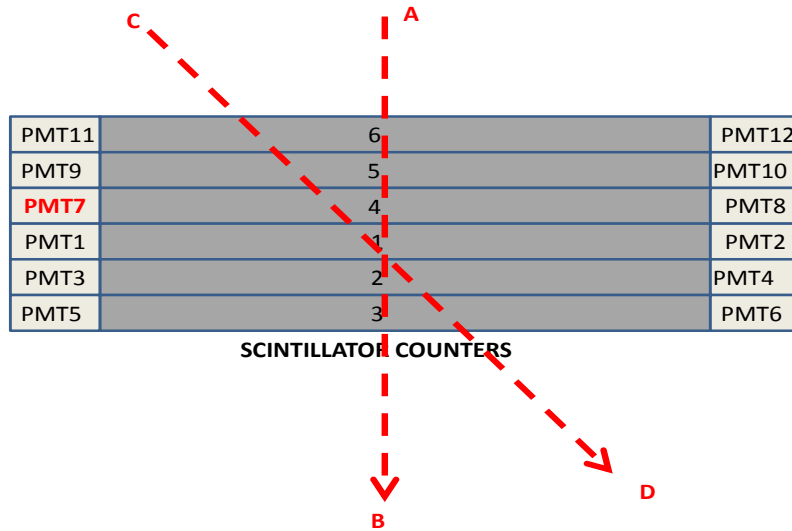
Figure 5.1: Scintillator counter test arrangement and the corresponding PMTs.

The scintillation sectors were arranged in a complementary order at JLab according to how they were built into the CLAS 12 detector as shown in Figure 5.1. AB and CD are the two paths which the cosmic rays can take while travelling through the counter arrangement. Path CD is the one when the rays travel a longer distance diagonally through the counters and hence they produce large PMT signals. As mentioned earlier in chapter 2 that the maximum charge that could be recorded in the 4 ns intervals is 400 pC, so the events which involve very flat paths produce FADC histograms with flat tops like in Figure 2.4. However these events are excluded in the timewalk analysis by a cut on the maximum allowed FADC fully integrated charge (1.7 nC).
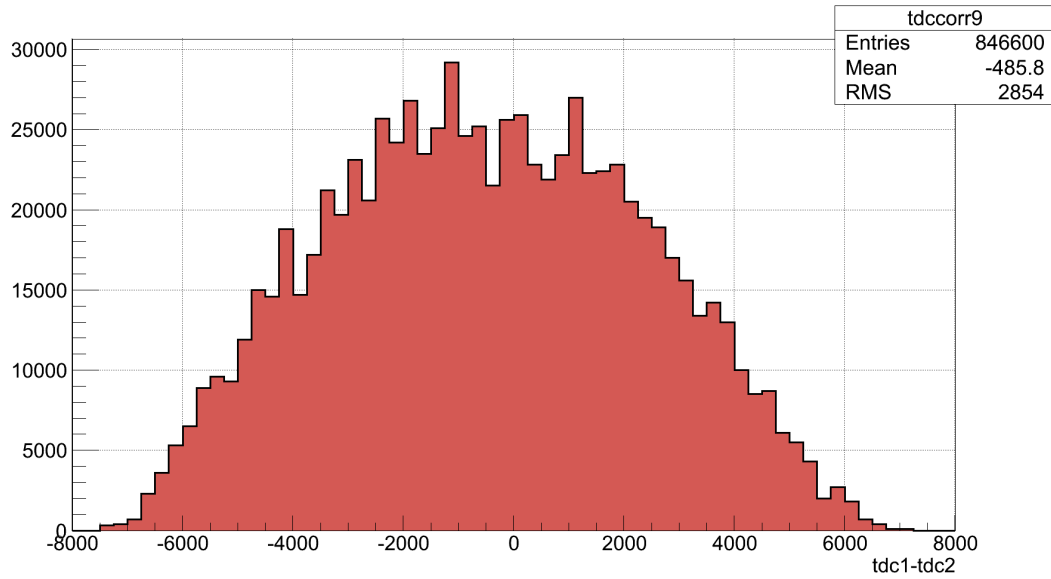
33

Figure 5.2: TDC difference tdc1-tdc2.

Figure 5.2 shows a one-dimensional histogram for the distribution of the differences in tdc1 and tdc2 values in ps (corresponding to PMT1 and PMT2) for all events. Referring to Figure 5.1, one can see that the PMT1 is on the left and PMT2 is on the right of the scintillation counter number 1. If an event is close to PMT1 then we get all negative values for TDC differences whereas if the event occurs near PMT2 then we get all positive values for TDC differences. If the event occurs at the middle of the scintillator counter then we get the TDC differences around 0, and so on.
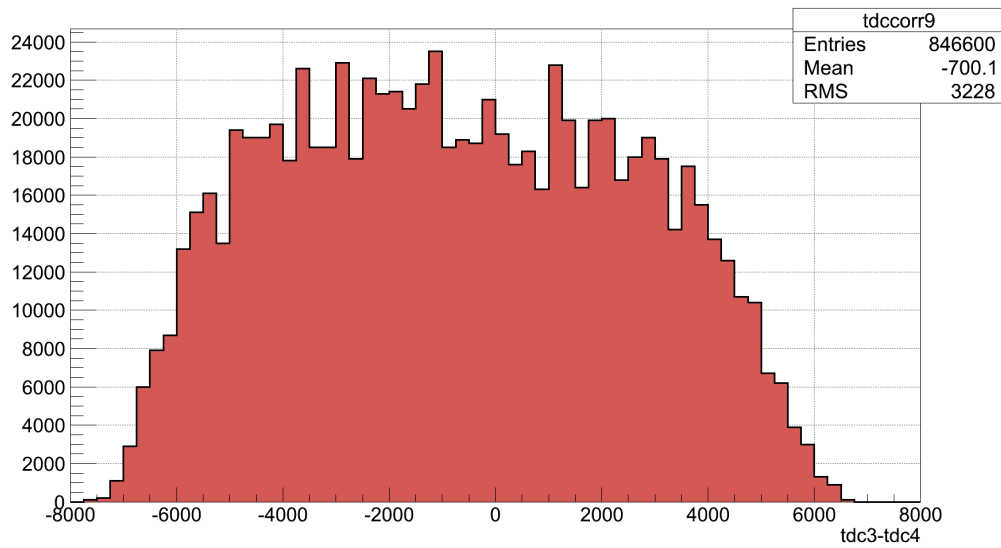
34

Figure 5.3: TDC difference tdc3-tdc4.

Figure 5.3 shows a one-dimensional histogram for the differences in tdc3 and tdc4 values (corresponding to PMT3 and PMT4) for all events. This histogram has the same logic as for Figure 5.3. PMT3 is on the left and PMT4 is on the right of the scintillation counter number 2.
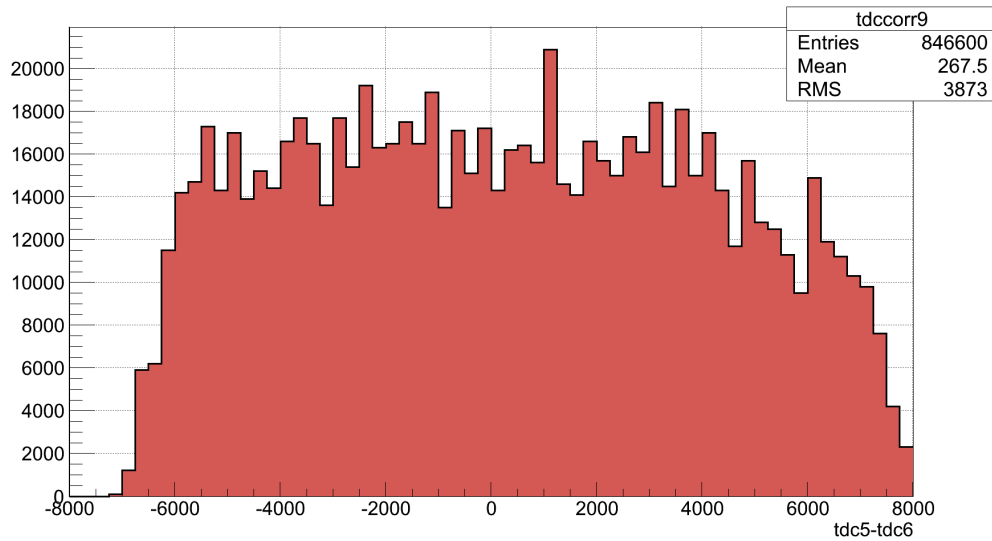
35

Figure 5.4: TDC difference tdc5-tdc6.

Figure 5.4 shows a one-dimensional histogram for the difference in tdc5 and tdc6

values (corresponding to PMT5 and PMT6) for all events. PMT5 is on the left and the

PMT6 is on the right of scintillator counter number 3. The histogram is "flatter" because

the scintillation counter 3 is on the edge (bottom bar) of the arrangement as shown in
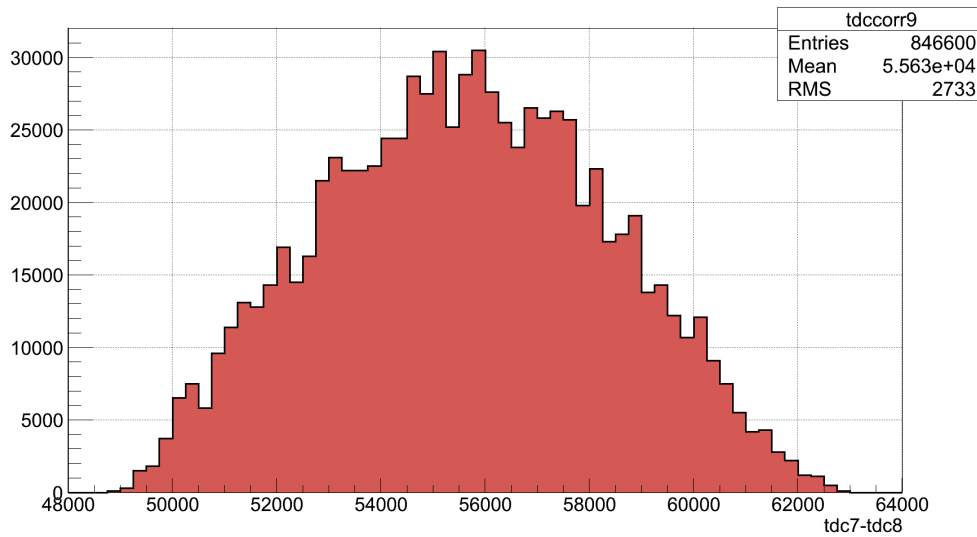
Figure 5.1.

Figure 5.5: TDC difference tdc7-tdc8.

Figure 5.5 shows a one-dimensional histogram for the difference in tdc7 and tdc8 values (corresponding to PMT7 and PMT8) for all events. PMT7 is on left and PMT8 is on the right of scintillator counter number 4. Figures 5.2, 5.3, 5.4 have the TDC difference distribution between -8000 to 8000. But in this case the distribution is between 48000 to 62000. This is because PMT7 is set to be the reference PMT and hence its timing is delayed as compared to other PMTs.

37

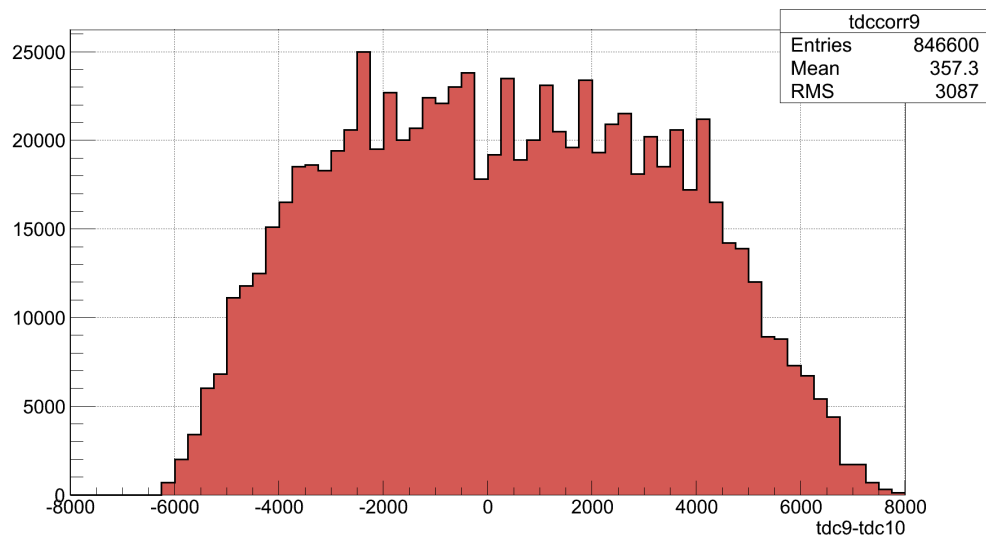| tdccorr9	
Entries	846600
Mean	357.3
RMS	3087

Figure 5.6: TDC difference tdc9-tdc10.

Figure 5.6 shows a one-dimensional histogram for the difference in tdc9 and tdc10 values (corresponding to PMT9 and PMT10) for all events. PMT9 is on the left and PMT10 is on the right of scintillator counter number 5.
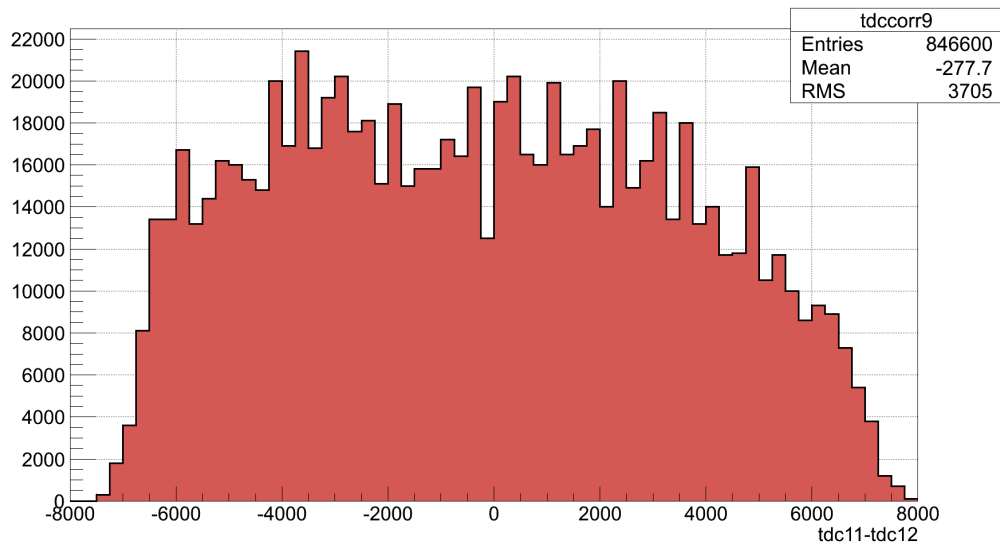
Figure 5.7: TDC difference tdc11-tdc12.

Figure 5.7 shows a one-dimensional histogram for the difference in tdc11 and tdc12 values (corresponding to PMT11 and PMT12) for all events. PMT11 is on the left and PMT12 is on the right of the scintillator counter number 6. The histogram in Figure 5.7 has again "flatter" distribution because counter 6 is on the edge (top bar) of the arrangement as shown in Figure 5.1.

Further two dimensional histograms are plotted to study the correlation between the TDCs. These correlation histograms help in studying where exactly the events has occurred along the scintillator bars.

39
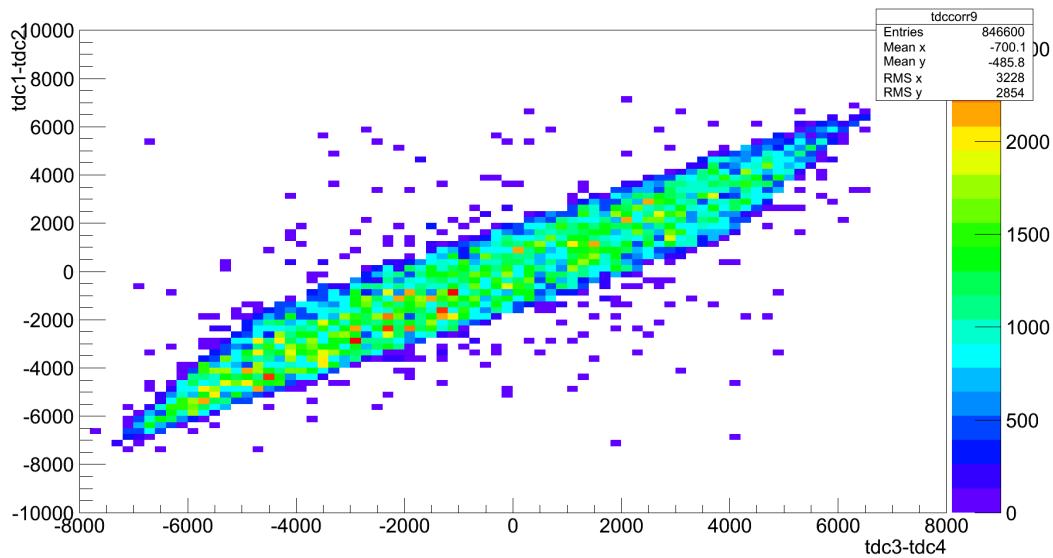
Figure 5.8: TDC correlation tdc1-tdc2 vs tdc3-tdc4.

Figure 5.8 show TDC correction between the counters 1 and 2. These two counters are placed next to each other and thus show a relatively strong correlation. Looking at the histogram, the data points around -6000 y-axis channels refer to the events closer to PMT1. In the same manner the data points around 8000 refer to events closer to PMT2. The distribution around 0 refers to the events at the center of the bars.
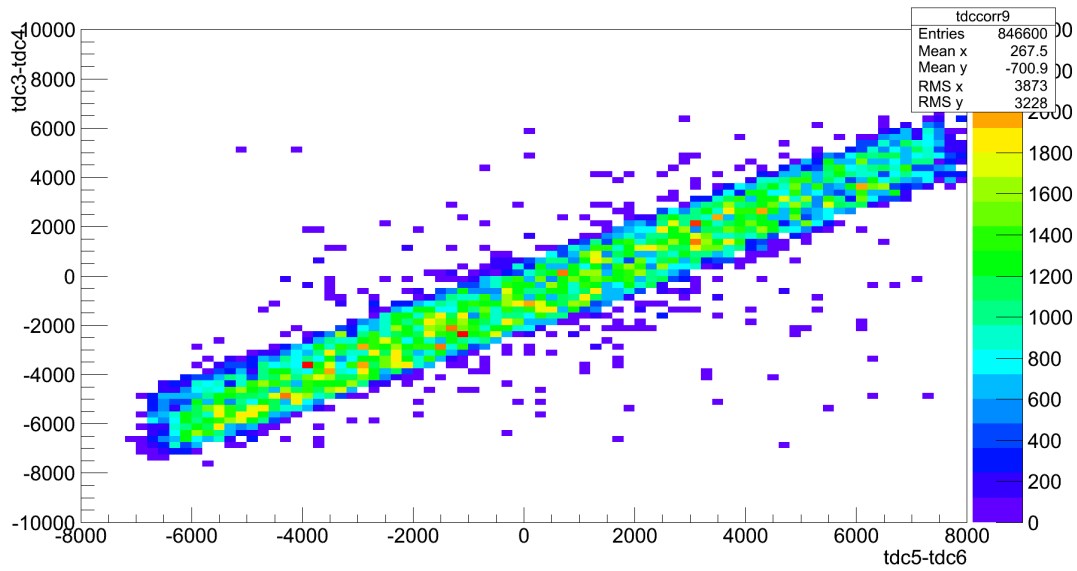
Figure 5.9: TDC correlation tdc3-tdc4 vs tdc5-tdc6.

These two counters are placed next to each other showing again a relatively strong correlation even without applying any further cuts. Similar logic applies in this case as well as in Figure 5.8. The position of red points (which refer to maximum occurrence) on the diagonal indicate that for more events the cosmic ray particle travelled vertically through the set up than under other angles.

41
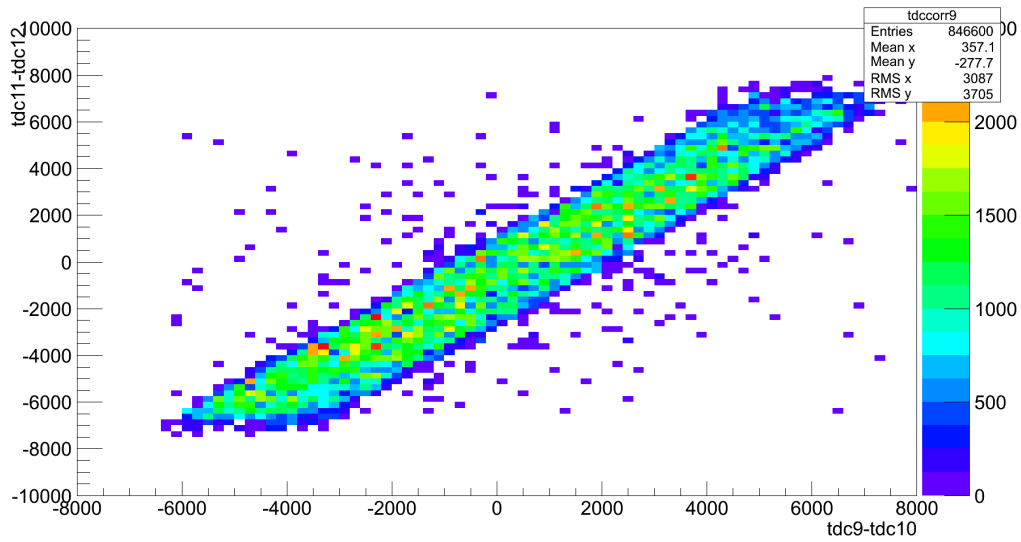
Figure 5.10: TDC correlation tdc11-tdc12 vs tdc9-tdc10.

Figure 5.10 refer to the counters 5 and 6. Again similar logic applies to all neighbouring

bars. Since the possibility of a diagonal path for the cosmic rays is reduced in the case of

neighbouring bars it can be concluded that majority of the rays rather followed a

vertical path like AB between these two counters.

Figure 5.11: TDC correlation tdc11-tdc12 vs tdc5-tdc6.

Figure 5.11 shows the TDC correlation between the counters on the edge of the

arrangement i.e counters 6 and 3.

www.manaraa.com
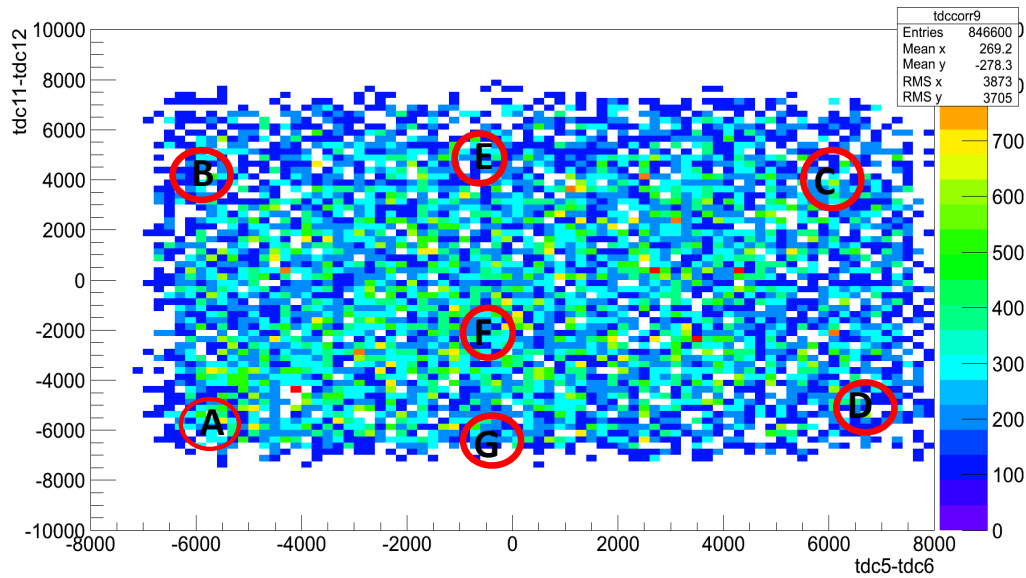
Figure 5.12: TDC correlation.

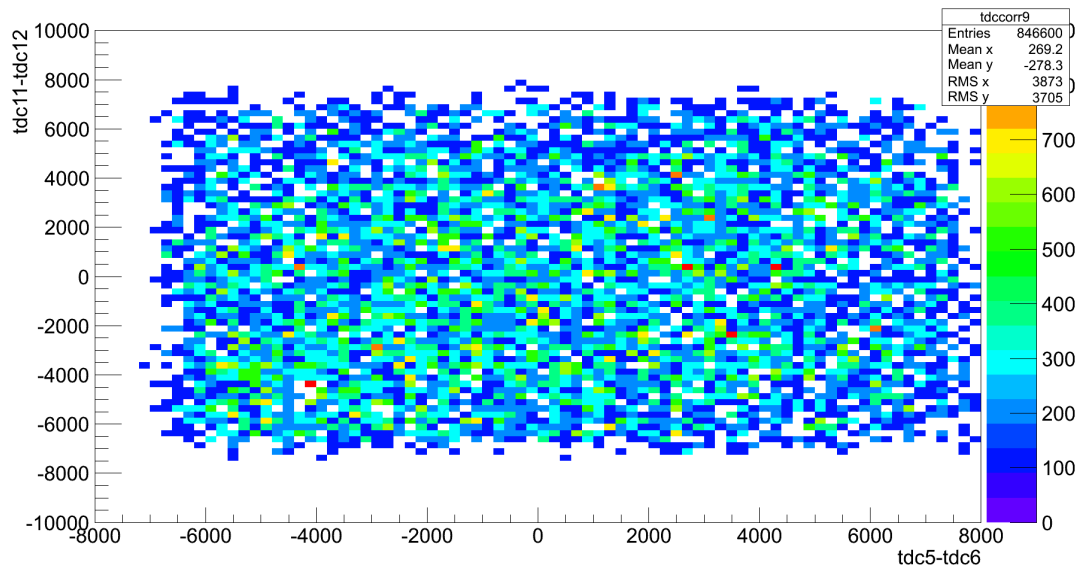In Figure 5.12 if events occur around point A, then they are close to the PMT5 and PMT11 on the left side of the counters. B and C indicate that the events are close to PMT12. D indicates that they are close to PMT6. E, F,G indicate that the events have occurred at the center of the bottom. Events lying along the diagonal A, F, C indicate that the cosmic ray has followed a vertical path AB as in Figure 5.1. Due to lack of statistics, a cut on the diagonal AEC that would isolate the vertical paths could not be applied.

44
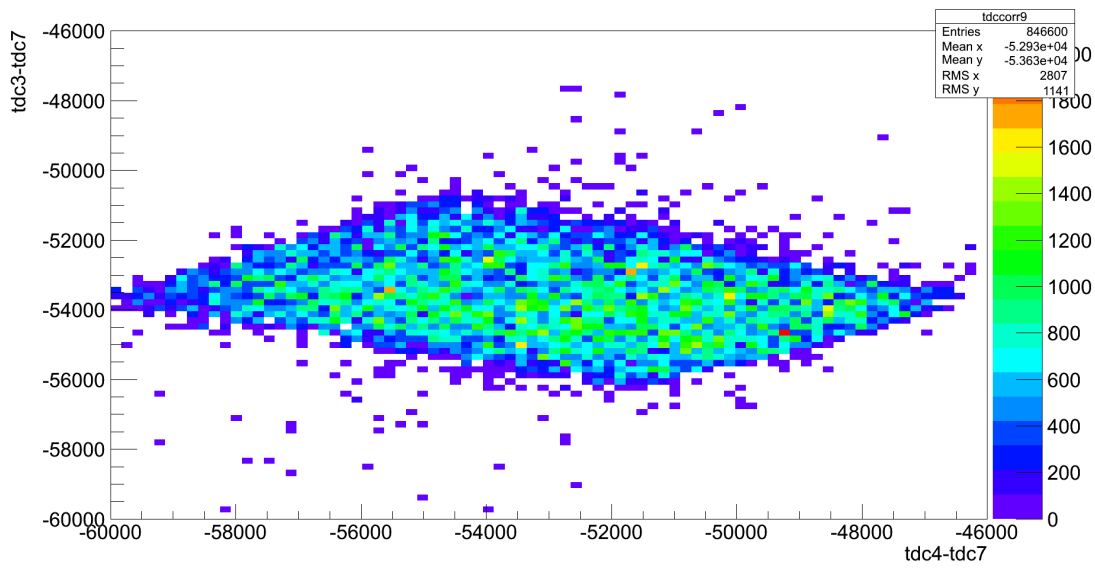
Figure 5.13: tdc3-tdc7 vs tdc4-tdc7.

In Figure 5.13 the TDC values of the reference PMT7 has been subtracted from the left PMT3 and right PMT4. Since the timing of the TDC7 is delayed, so subtracting the tdc7 values from tdc3 and tdc4 gives the distribution along the negative x-axis and y-axis channels.
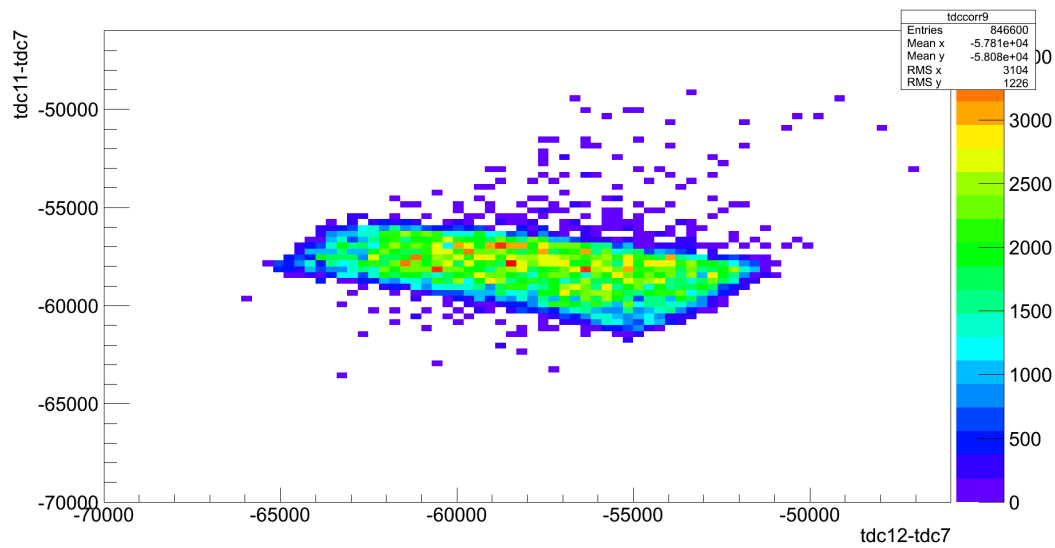
Figure 5.14: tdc11-tdc7 vs tdc12-tdc7.

 Figures 5.13 and 5.14 were plotted mainly to confirm that the PMT7 serves as the

reference PMT.

Chapter 6: Timewalk correction and time resolution

To mitigate the effect of timewalk on the measurement of time resolution using three-bar cosmic ray method (see Figure 6.1), a one parameter timewalk correction is applied to each PMT. The middle left PMT marked as PMT ML (middle left) is taken to be the reference PMT. The reference PMT determines the relative timing of all other signals. For a single relative time

$t_{corrected} = (TDC_i + TWC_i)$

where $t_{corrected}$ is the timewalk corrected time for the PMT. TDC_i is the TDC value for the corresponding PMT_i. TWC_i is the difference between the maximum amplitude and the threshold point and hence the timewalk correction value (see Figure 4.11).

As mentioned earlier, the three-bar cosmic ray method has been used for the measurement of the time resolution. As referred to *Ralf Gothe, 2009[2]* "the three bar cosmic ray method has three primary advantages: a high event rate, a symmetry that allows for the collective treatment of all particle paths, and an energy deposit per particle similar to the CLAS12 experimental conditions." The three-bar cosmic ray configuration has three identical equally spaced counters and each counter contributes equally to the overall time resolution.

47
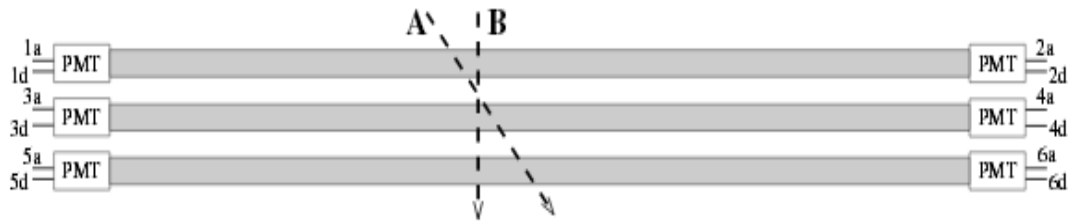
Figure 6.1: Counter arrangement for the three-bar cosmic ray method.

According to **Ralf Gothe, 2009[2]** Figure 6.1 shows the configuration of the counters

and two possible paths A and B of ionizing particles. The three counters are equally

spaced so that the path between the top and the bottom counters is bisected by the

middle counter which guarantees that

$$T \equiv \frac{t_t + t_b}{2} - t_m = const$$

i.e. T is independent of the path traversed by the particle. t_t, t_m and t_b denote the

individual times of the particle registered by the top, middle and the bottom, counters

respectively.

These three times are determined as follows

$$t_t = \frac{t_{tl} + t_{tr}}{2} = \frac{t_1 + t_2 - 2t_{ref}}{2}$$
$$t_m = \frac{t_{ml} + t_{mr}}{2} = \frac{t_3 + t_4 - 2t_{ref}}{2}$$
$$t_b = \frac{t_{bl} + t_{br}}{2} = \frac{t_5 + t_6 - 2t_{ref}}{2}$$

7

t_{ref} is the reference time. Eventually, the reference time cancel out in the final

expression for T[8].

$$T = \frac{t_1 + t_2 + t_5 + t_6 - 4t_{ref}}{4} - \frac{t_3 + t_4 - 2t_{ref}}{2}$$
$$= \frac{t_1 + t_2 + t_5 + t_6}{4} - \frac{t_3 + t_4}{2}$$

---

[7] The expressions are taken from Ralf Gothe[2]
[8] The expressions are taken from Ralf Gothe[2]

49

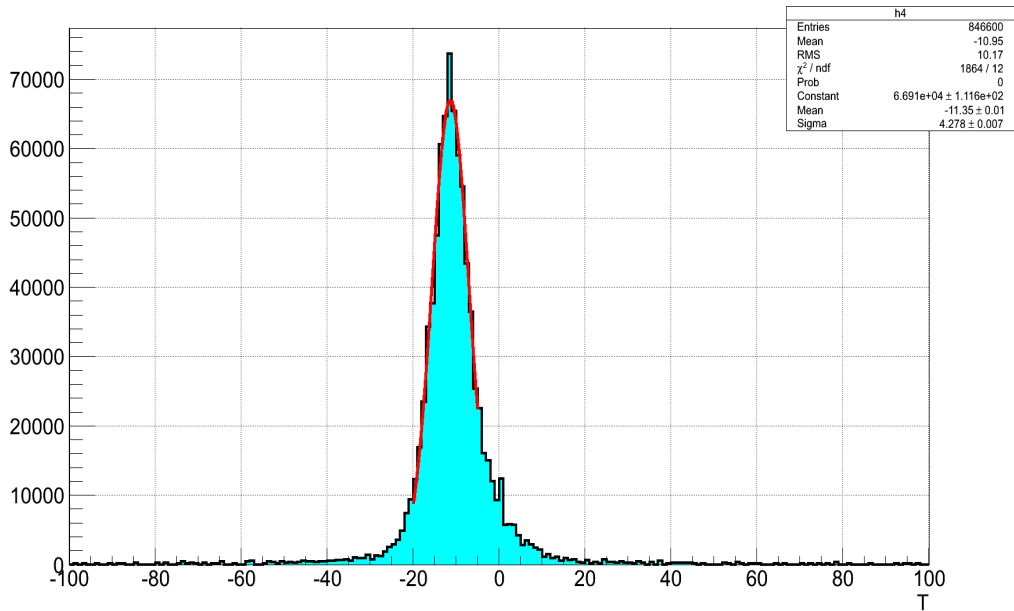| h4	
Entries	846600
Mean	-10.95
RMS	10.17
χ^2 / ndf	1864 / 12
Prob	0
Constant	6.691e+04 ± 1.116e+02
Mean	-11.35 ± 0.01
Sigma	4.278 ± 0.007

Figure 6.2: Uncorrected spread of T.

Figure 6.1 shows the uncorrected spread of T with sigma of 4.278 bins. Across the entire 94.13 cm length of the identical counter, the resolution is hence

$\sigma_T = \sqrt{2/3}$(4.278 bins * 25 ps/bin)= 87.32 ps[9]

According to **Ralf Gothe, 2009[2]** the spreading of T is quantified by its standard deviation σ_T , and its related to σ_i which is the standard deviation of time measurements from each PMT i by σ_T^2= 1/16 (σ_1^2 +σ_2^2 +σ_5^2+ σ_6^2)+ 1/4 (σ_3^2 +σ_4^2) .

Each counter is composed of a scintiallation counter and two identical PMTs. This justifies the assumption that each of the two time measurements from one counter would contribute equally to the resolution of the counter, i.e. $\sigma_{1,2}$ = σ_1 = σ_2 and $\sigma_{3,4}$ = σ_3 = σ_4 and $\sigma_{5,6}$ = σ_5 = σ_6.

---

[9] The factor $\sqrt{2/3}$ comes when all the three bars are treated as identical i.e σ_m=σ_T=σ_r and thus σ_m=$\sqrt{\frac{2}{3}}$ σ_T

50

If only the counters the top and the bottom are identical and thus $\sigma_{1,2} = \sigma_{5,6}$. Since $\sigma_{counter} = 1/\sqrt{2} \ \sigma_{PMT}$, the resolution of the middle counter is detrained in terms of the measured σ_T and the known resolution $\sigma_r = 1/\sqrt{2} \ \sigma_{1,2}$ of each of the reference counters

$$\sigma_T^2 = \frac{1}{16}4\sigma_{1,2}^2 + \frac{1}{4}2\sigma_{3,4}^2$$

$$\sigma_T^2 = \frac{1}{16}4(\sqrt{2}\sigma_r)^2 + \frac{1}{4}2(\sqrt{2}\sigma_m)^2$$

$$\sigma_T^2 = \frac{1}{2}\sigma_r^2 + \sigma_m^2$$

$$\sigma_m = \sqrt{\sigma_T^2 - \frac{1}{2}\sigma_r^2}$$

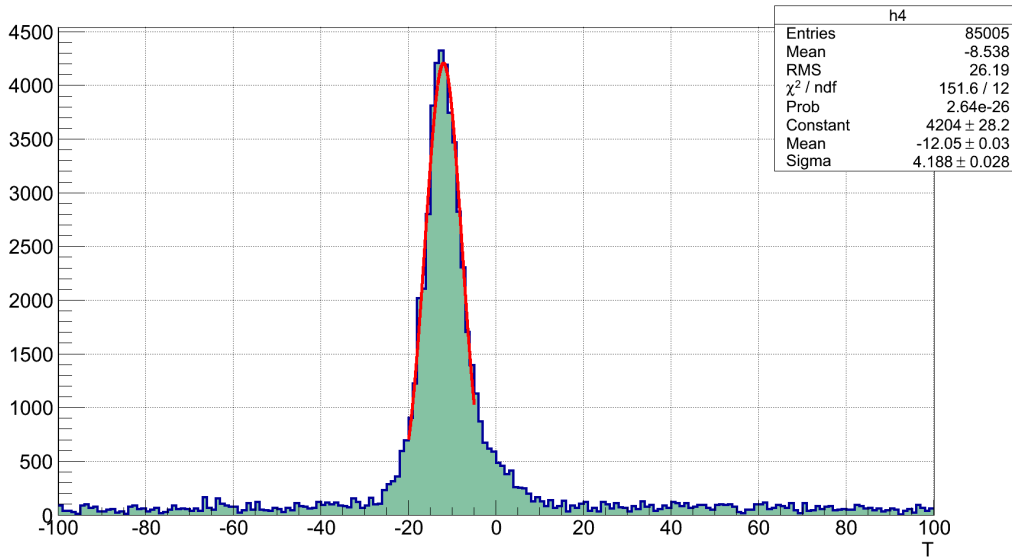| h4	
Entries	85005
Mean	-8.538
RMS	26.19
χ^2 / ndf	151.6 / 12
Prob	2.64e-26
Constant	4204 ± 28.2
Mean	-12.05 ± 0.03
Sigma	4.188 ± 0.028

Figure 6.3: Corrected spread of T.

Figure 6.3 shows the timewalk corrected spread of T with sigma of 4.188 bins. Across the entire 94.13 cm length of the identical counter, the resolution is hence

$\sigma_T = \sqrt{2/3}$(4.188 bins * 25 ps/bin)= 85.4 ps. The time resolution after timewalk correction had little difference from the uncorrected resolution (87 ps).
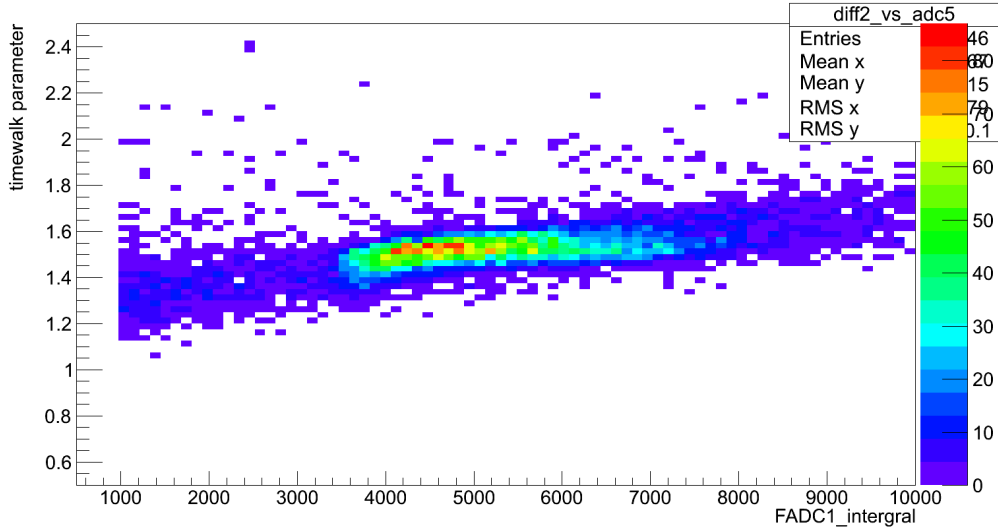
51

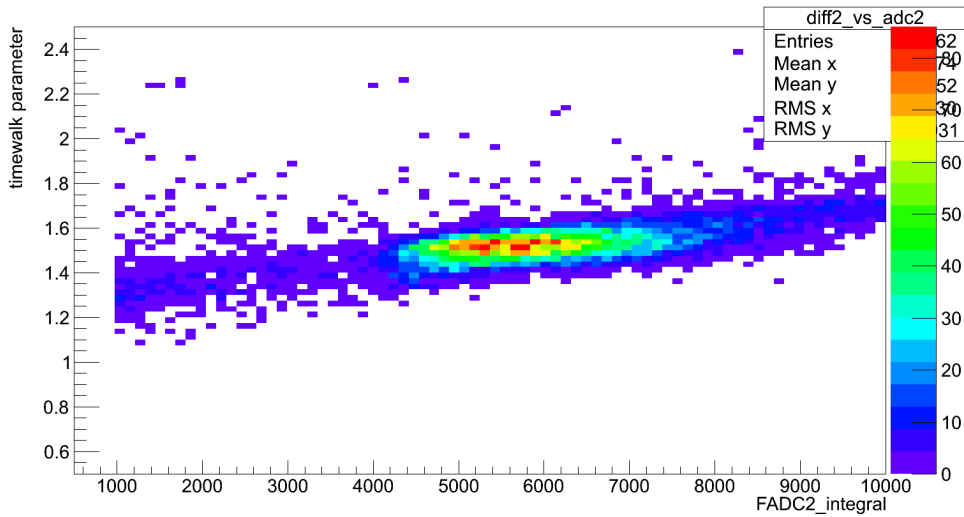**Figure 6.4: Timewalk parameter vs FADC1_integral.**

Figure 6.5: Timewalk parameter vs FADC2_integral.

Figures 6.4 and 6.5 show the histogram plotted between timewalk parameters and the

full integral vales of the FADCs. The two histograms are consistent. From these two

histograms it could be justified that the resolution of the histograms in Figures 6.4 and

52

6.5 are of the same order of about 100 ps as compared with the resolution of the histogram in Figure 6.3 (4.188 * 25 ps= 104.5). Figures 6.4 and 6.5 illustrates a wide spread of timewalk parameters and hence large uncertainty in the timewalk correction values. Dur to this large uncertainty the timewalk correction did not show any significant effect on the time resolution in Figure 6.3. However with higher frequency of the FADC, there would be more points for which the fits on the histograms would be stable and would provide better resolution with timewalk correction. In this case the clock frequency of 250 MHz was not enough to produce significant effect on the time resolution with timewalk correction.

Conclusion

The TOF upgrade at 12 GeV requires particle identification upto higher momenta and hence better charged particle time resolution. This thesis was focussed on comparing the time resolution measurements based on timewalk corrections obtained from the FADC250 with the previously measured time resolution as in the comprehensive update by *Ralf Gothe[2]* obtained with the standard timewalk correction. The timewalk uncorrected time resolution is measured to be 87.32 ps with bar length of 94.13 cm as compared to the timewalk uncorrected time resolution of 86.6 ps (refer *Ralf Gothe[2]*) with bar length of 120-cm. The timewalk corrected resolution measured is 85.4 ps. The timewalk correction with FADC250 did not show significant improvement on the time resolution. The standard time resolution measured as in *Ralf Gothe[2]* is 42.6 ps. Using FADC with higher frequency could provide better results since there would be more number of points providing a stable fit on the histograms and thus the timewalk-corrected time resolution would be better.

References

[1] D.S. Carman, "Forward Time-of-Fight Geometry for CLAS12", Jefferson

Laboratory, ftof_geom.tex, November 15,2013

[2] Ralf Gothe, Evan Phelps, Robert Steinman, and Ye Tian," CLAS12

Forward Time-of-Flight at USC: A Comprehensive Update", Department of

Physics and Astronomy, University of South Carolina, November 21, 2009.

[3] FIRMWARE for FADC250 Ver2 ADC FPGA, manual